

Theory of tunneling spectroscopy in p -wave altermagnet-superconductor hybrid structures

Kazuki Maeda,¹ Bo Lu,² Keiji Yada,¹ and Yukio Tanaka¹

¹*Department of Applied Physics, Nagoya University, Nagoya 464-8603, Japan*

²*Department of Physics, Tianjin University, Tianjin 300072, China*

(Dated: July 8, 2024)

Abstract

We theoretically study the tunneling conductance of a junction consisting of a two-dimensional p -wave altermagnet (AM) and a superconductor (SC) for various pairing symmetries. The zero bias conductance peaks arising from the dispersionless surface Andreev bound states (SABSs) in d_{xy} -wave and p_x -wave superconductor junctions are insensitive against varying the altermagnetic spin-splitting strength α_y . Moreover, for chiral p - or chiral d -wave SCs, zero bias conductance shows a non-monotonic change as a function of α_y indicating the existence of the dispersive SABSs. Our obtained results of tunneling spectroscopy based on a p -wave AM serve as an effective way for the identification of the pairing symmetries of unconventional superconductors. It is noted that our used Hamiltonian of AM is also available for persistent spin helix systems.

I. INTRODUCTION

Altermagnets (AMs)¹⁻⁸ are an emerging class of magnetic materials as a third magnetic phase beyond ferromagnets (FMs) and antiferromagnets (AFMs). AMs are distinct from FMs in the sense that AMs have vanishing macroscopic magnetism. Instead, AMs possess alternating spin-polarized magnetic order in the momentum space in contrast with the spatially varying order in AFMs. Candidate AM materials include RuO₂^{2,9,10}, MnTe¹¹⁻¹³, Mn₅Si₃¹⁴ as well as semiconductors/insulators like MnF₂ and La₂CuO₄¹⁵.

In this context, the interplay between superconductor (SC) and AMs in heterostructures¹⁶⁻²² is of particular interest since AMs could make it possible to fabricate superconducting spintronic devices discussed in ferromagnet / superconductor (FM/SC) junctions²³⁻²⁶ with zero net magnetism. In FM/SC junctions, the spin-polarized field in ferromagnets makes the alignment of electron spins and generally suppresses the formation of Cooper pairs near the junction boundaries. Nevertheless, AMs may overcome the difficulty of the coexistence of exchange field and pair potential, e.g., with reduced stray field²⁷. Moreover, several proposals have been formulated to realize topological superconductors in the proximitized altermagnet systems^{28,29}.

Although antiferromagnet / superconductor (AFM/SC) junctions also exhibit anomalous features arising from e.g., so-called Q reflection³⁰⁻³³ with reduced stray field, AM/SC junctions could show distinguished features due to spin-splitting in the momentum space.

On the other hand, to study Andreev reflection and charge transport in SC junction has been a very fundamental problem in superconductivity³⁴. It is known that the Andreev reflection and charge conductance depend significantly on both spin-splitting fields and unconventional pairings. The former factor indicates that Andreev reflection is a spin-sensitive process and the latter usually gives rise to the surface Andreev bound states (SABSs) resulting in the enhanced Andreev probabilities^{35,36}. When pair potential has a line or point nodes, the topological invariant can be defined in the Brillouin zone and it leads to the flat-band zero energy SABS (ZESABS) or dispersive SABSs³⁷⁻⁴⁵. In the case of spin-singlet d -wave SCs or spin-triplet p -wave SC with line nodes, a zero bias conductance peak (ZBCP) appears in normal metal/SC junctions^{35,36,46,47} due to the presence of ZESABS^{47,48}. The ZBCP was experimentally observed in tunneling spectroscopy on high T_c cuprate^{47,49-57}. Also, the study of FM / unconventional SC junctions have been studied both for spin-singlet

d -wave^{58–60} and spin-triplet p -wave SCs⁶¹. Basically, the Andreev reflection and the height of ZBCP are suppressed by the exchange field in FM / d -wave SC. On the other hand, in spin-triplet junctions, the influence FM depends on the relative directions between the exchange field and d -vector of spin-triplet pairing⁶².

Based on these backgrounds of the tunneling spectroscopy, studying Andreev reflection and charge transport in AM/SC junctions for various pairing symmetry becomes an interesting topic. The transport study of AM/SC junctions indicates a variety of new phenomena. In an AM/ s -wave SC junction, studies show that Andreev reflection is sensitive to both the crystal orientation and the strength of the spin-splitting field^{17,18}, as compared to ferromagnetic materials which are orientationally independent. The study also shows that the zero-biased conductance peak is still prominent in the tunneling spectroscopy of an AM/ d -wave SC junction. Interestingly, AM can display $0 - \pi$ oscillations in the Josephson junction without net magnetism^{19,20,22}. It is also noted that the symmetry of the AM is restricted to d -wave in the previous studies of AM/SC junctions. Recent research has shown a variety of other possibilities of symmetries of altermagnetism, such as p -wave AM. Altermagnetism is different from Dirac spin-orbit coupling in that Dirac spin-orbit interaction is a weak interaction that appears in the order of $1/c^2$ expansion of the Dirac equation while AM appears in the non-relativistic limit⁶³. While it has been predicted that even-parity-wave collinear magnetism like d -wave AM can be realized in many kinds of materials, the realization of stable p -wave AM was recently proposed in a non-coplanar magnetic structure⁶³. Thus, it is worth studying Andreev reflection beside d -wave AM and exploring extensive pairings in the transport property of AM/SC junctions. Here, we study this problem based on an effective model of p -wave altermagnet which has been used as a model of persistent spin-helix^{64–70}.

The organization of this paper is as follows. In section II, we explain the model and the theoretical formulation. We obtain the conductance formula analytically. In section III, we show the tunneling conductance between AM /SC junctions by changing the pairing symmetry in SC. We choose s -wave, $d_{x^2-y^2}$ -wave, d_{xy} -wave, p_x -wave, p_y -wave, chiral p -wave, and chiral d -wave pairings. The flat band ZESABS appears for d_{xy} -wave and p_x -wave pairings and chiral p -wave and chiral d -wave pairings have dispersive SABS. We also study the impact of ferromagnetic insulators at the interface in the AM/SC junctions. In section IV, we summarized the obtained results.

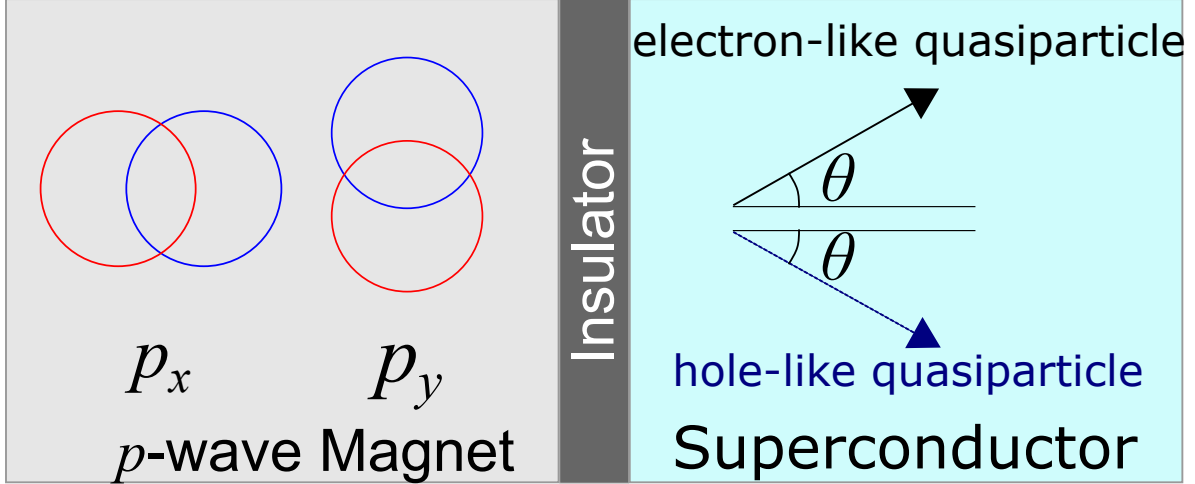


FIG. 1. Schematic illustration of p -wave altermagnet/Insulator/Superconductor junction. The angle θ corresponds to the direction of the electron-like quasiparticle in SC measured from the normal to the interface.

II. MODEL AND FORMULATION

In this section, we consider a p -wave AM / Insulator (I) / SC junction as shown in Fig. 1. The corresponding Bogoliubov-de Gennes (BdG) Hamiltonian in the system can be written by 4×4 matrix as follows:

$$\check{\mathcal{H}}_{\text{BdG}} = \begin{bmatrix} \hat{h}(\mathbf{k}, x) & \hat{\Delta}(\hat{\mathbf{k}}) \Theta(x) \\ -\hat{\Delta}^*(-\hat{\mathbf{k}}) \Theta(x) & -\hat{h}^*(-\mathbf{k}, x) \end{bmatrix} \quad (1)$$

where $\hat{h}(\mathbf{k}, x)$ is a single-particle Hamiltonian

$$\hat{h}(\mathbf{k}, x) = \text{diag}(\xi_+(\mathbf{k}, x), \xi_-(\mathbf{k}, x)) + \hat{U}_0 \delta(x) \quad (2)$$

$$\xi_{\pm}(\mathbf{k}, x) = (\mathbf{k} \pm \boldsymbol{\alpha} \Theta(-x))^\top \frac{\hbar^2}{2m} (\mathbf{k} \pm \boldsymbol{\alpha} \Theta(-x)) - \mu \quad (3)$$

with a momentum $\mathbf{k} = -i\nabla$, the effective mass of an electron m , and the chemical potential μ . It is noted that we employ Eq. (3) to describe p -AM, exhibiting the same shape of Fermi surface and the sign of S_z component given in Ref.⁶³. Here, 2×2 matrix \hat{U}_0 given by

$$\hat{U}_0 = \text{diag}(U_\uparrow, U_\downarrow) \quad (4)$$

denotes the flat insulating barrier at $x = 0$. $\Theta(x)$ is the Heaviside step function.

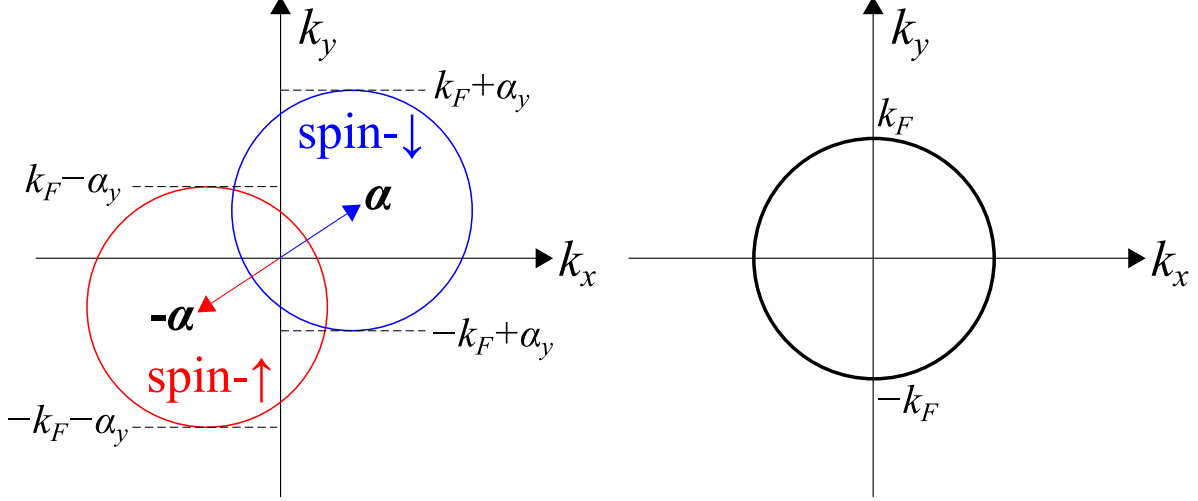


FIG. 2. Schematic illustration of the Fermi surfaces in p -wave altermagnet (AM, left panel) and superconductor (SC, right panel). The magnitude and the direction of the splitting of the Fermi surface in AM are described by α vector.

Here, the Fermi surfaces for spin- \uparrow and spin- \downarrow electrons in AM are split as shown in Fig. 2 by α vector. It is noted that the present Hamiltonian of p -wave AM is essentially equivalent to the Hamiltonian of persistent helix⁶⁴⁻⁷³. The Nambu spinor $\Psi(x, y) = [u_\uparrow, u_\downarrow, v_\uparrow, v_\downarrow]^\top$ on the field operator basis $[\psi_\uparrow, \psi_\downarrow, \psi_\uparrow^\dagger, \psi_\downarrow^\dagger]^\top$ follows the BdG equation

$$\check{\mathcal{H}}_{\text{BdG}}\Psi = E\Psi \quad (5)$$

In the SC region $x > 0$, the pair potential is written as

$$\hat{\Delta}(\pm\hat{\mathbf{k}}) = \begin{bmatrix} 0 & \Delta(\theta) \\ -\Delta(\theta) & 0 \end{bmatrix} \quad (6)$$

$$\hat{\mathbf{k}} = \frac{\mathbf{k}}{|\mathbf{k}|} \quad (7)$$

$$\theta = \arctan \frac{k_y}{k_x} \quad (8)$$

for spin-singlet SC, or

$$\hat{\Delta}(\pm\hat{\mathbf{k}}) = \pm \begin{bmatrix} 0 & \Delta(\theta) \\ \Delta(\theta) & 0 \end{bmatrix} \quad (9)$$

for spin-triplet SC with a \mathbf{d} vector parallel to the z -axis, or the Néel vector of the AM, which corresponds to the Cooper pair with the z -component of spin $S_z = 0$. The y -component of

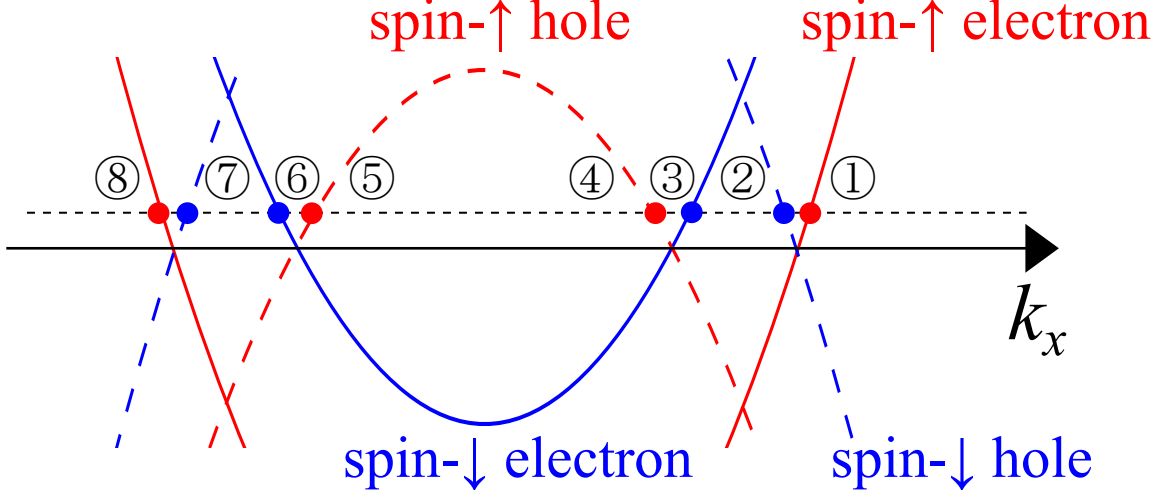


FIG. 3. Schematic illustration of the dispersion relation in p_y -wave AM for $\alpha_y k_y < 0$. The points ①–⑧ correspond to $k_{e\uparrow}^+, k_{h\downarrow}^-, k_{e\downarrow}^+, k_{h\uparrow}^-, k_{h\uparrow}^+, k_{e\downarrow}^-, k_{h\downarrow}^+$, and $k_{e\uparrow}^-$, respectively.

the wave vector k_y is preserved and the wave function can be written as

$$\Psi_\rho(x, y) = \Psi_\rho(x, k_y) e^{ik_y y}. \quad (10)$$

The boundary conditions of the wave function at $x = 0$ are written as

$$\Psi_\rho(x, k_y) \Big|_{x=0_+} = \Psi_\rho(x, k_y) \Big|_{x=0_-}, \quad (11)$$

$$\check{v}_x \Psi_\rho(x, k_y) \Big|_{x=0_+} - \check{v}_x \Psi_\rho(x, k_y) \Big|_{x=0_-} = \frac{2}{i\hbar} \left(\hat{I} \otimes \hat{U}_0 \right) \check{\tau}_z \Psi_\rho(0, k_y), \quad (12)$$

where 4×4 matrix \check{v}_x is a velocity operator given by

$$\check{v}_x = \frac{1}{\hbar} \frac{\partial \check{\mathcal{H}}_{\text{BdG}}}{\partial k_x} = \frac{\hbar}{m} \left(\check{\tau}_z \frac{1}{i} \frac{\partial}{\partial x} + \check{\sigma}_z \alpha_x \Theta(-x) \right), \quad (13)$$

with

$$\hat{I} = \text{diag}(1, 1), \quad \check{\tau}_z = \text{diag}(1, 1, -1, -1), \quad \check{\sigma}_z = \text{diag}(1, -1, 1, -1). \quad (14)$$

In the SC region $x < 0$, we derived the expression of the wave functions based on the standard theory of tunneling spectroscopy of unconventional superconductors⁴⁷ (see Appendix A.)

In the AM region $x < 0$, the x -components of the possible wave vectors for fixed E and k_y are given by

$$k_{e\uparrow}^{\pm} = -\alpha_x \pm \sqrt{\frac{2m}{\hbar^2} (E + \mu) - (k_y + \alpha_y)^2}, \quad (15)$$

$$k_{e\downarrow}^{\pm} = \alpha_x \pm \sqrt{\frac{2m}{\hbar^2} (E + \mu) - (k_y - \alpha_y)^2}, \quad (16)$$

$$k_{h\uparrow}^{\pm} = \alpha_x \mp \sqrt{\frac{2m}{\hbar^2} (-E + \mu) - (k_y - \alpha_y)^2}, \quad (17)$$

$$k_{h\downarrow}^{\pm} = -\alpha_x \mp \sqrt{\frac{2m}{\hbar^2} (-E + \mu) - (k_y + \alpha_y)^2}, \quad (18)$$

where the subscripts e and h correspond to an electron and a hole respectively, \uparrow, \downarrow denote the spin, and the superscripts \pm correspond to the sign of the eigenvalues of \tilde{v}_x . For spin- \uparrow electron injection from $x < 0$, the wave function in AM can be written as

$$\Psi_{\uparrow}(x, k_y) = \begin{pmatrix} 1 \\ 0 \\ 0 \\ 0 \end{pmatrix} e^{ik_{e\uparrow}^+ x} + r_{\uparrow} \begin{pmatrix} 1 \\ 0 \\ 0 \\ 0 \end{pmatrix} e^{ik_{e\uparrow}^- x} + r_{\uparrow}^A \begin{pmatrix} 0 \\ 0 \\ 0 \\ 1 \end{pmatrix} e^{ik_{h\downarrow}^- x} \quad (19)$$

and that in SC can be written as Eq. (A1). In the same way, for spin- \downarrow electron injection, the corresponding wave function in AM can be written as

$$\Psi_{\downarrow}(x, k_y) = \begin{pmatrix} 0 \\ 1 \\ 0 \\ 0 \end{pmatrix} e^{ik_{e\downarrow}^+ x} + r_{\downarrow} \begin{pmatrix} 0 \\ 1 \\ 0 \\ 0 \end{pmatrix} e^{ik_{e\downarrow}^- x} + r_{\downarrow}^A \begin{pmatrix} 0 \\ 0 \\ 1 \\ 0 \end{pmatrix} e^{ik_{h\uparrow}^- x} \quad (20)$$

and in SC as given in Eq. (A2). Fig. 3 shows the dispersion relation and the x -components of the wave vectors in p_y -wave AM with $\boldsymbol{\alpha} \parallel \hat{\mathbf{y}}$. We see that the absolute value of the x -component of the velocity is approximately the same for a spin- \uparrow (\downarrow) electron and a spin- \downarrow (\uparrow) hole for $|E| \ll \mu$. It is noted that α_x only shifts the curves in Fig. 3 in the k_x -direction and does not affect the values of the x -components of the velocity.

For spin- ρ ($\rho = \uparrow, \downarrow$) electron injection with particular k_y , the particle flow

$$j_{\rho} = \text{Re}(\Psi_{\rho}^{\dagger} \tilde{v}_x \tilde{\tau}_z \Psi_{\rho}) \quad (21)$$

is preserved. We can obtain the transparency for spin- \uparrow electron injection

$$\sigma_{\uparrow}^S(E, k_y) = 1 + \operatorname{Re} \left(\frac{q_{e\uparrow}^-}{q_{e\uparrow}^+} \right) |r_{\uparrow}|^2 - \operatorname{Re} \left(\frac{q_{h\downarrow}^-}{q_{e\uparrow}^+} \right) |r_{\uparrow}^A|^2 \quad (22)$$

dividing Eq. (21) by the flow of the injection wave. In the same way, the transparency for spin- \downarrow electron injection becomes

$$\sigma_{\downarrow}^S(E, k_y) = 1 + \operatorname{Re} \left(\frac{q_{e\downarrow}^-}{q_{e\downarrow}^+} \right) |r_{\downarrow}|^2 - \operatorname{Re} \left(\frac{q_{h\uparrow}^-}{q_{e\downarrow}^+} \right) |r_{\downarrow}^A|^2 \quad (23)$$

Here,

$$q_{e\uparrow}^{\pm} = k_{e\uparrow}^{\pm} + \alpha_x, q_{e\downarrow}^{\pm} = k_{e\downarrow}^{\pm} - \alpha_x, q_{h\uparrow}^{\pm} = -k_{h\uparrow}^{\pm} + \alpha_x, q_{h\downarrow}^{\pm} = -k_{h\downarrow}^{\pm} - \alpha_x \quad (24)$$

We can also obtain the transparency for normal metal state $\sigma_{\uparrow}^N(E, k_y), \sigma_{\downarrow}^N(E, k_y)$ by substituting $\Delta(\theta) = 0$.

The differential conductance normalized by that for the normal metal state as a function of eV with bias voltage V can be written as,

$$\frac{G}{G_0} = \frac{\int_{-k_{F0}}^{k_{F0}} dk_y [\sigma_{\uparrow}^S(E, k_y) + \sigma_{\downarrow}^S(E, k_y)]}{\int_{-k_{F0}}^{k_{F0}} dk_y [\sigma_{\uparrow}^N(E, k_y) + \sigma_{\downarrow}^N(E, k_y)]}, \quad (25)$$

with $E = eV$. Note that when $q_{e\uparrow}^+$ ($q_{e\downarrow}^+$) becomes a purely imaginary number, it is natural to assume $\sigma_{\uparrow}^S(E, k_y) = \sigma_{\uparrow}^N(E, k_y) = 0$ ($\sigma_{\downarrow}^S(E, k_y) = \sigma_{\downarrow}^N(E, k_y) = 0$) since there is no traveling wave. It is noted that $\sigma_{\uparrow(\downarrow)}^S(E, k_y)$ and $\sigma_{\uparrow(\downarrow)}^N(E, k_y)$ are independent of α_x (see Appendix B).

Now, we assume that $E, |\Delta(\theta_{\pm})| \ll \mu$ following quasiclassical approximation^{35,47},

$$q_{e\uparrow}^+ \approx -q_{e\uparrow}^- \approx -q_{h\downarrow}^- \approx q_{\uparrow}^{\text{AM}} = \sqrt{\frac{2m\mu}{\hbar^2} - (k_y + \alpha_y)^2}, \quad (26)$$

$$q_{e\downarrow}^+ \approx -q_{e\downarrow}^- \approx -q_{h\uparrow}^- \approx q_{\downarrow}^{\text{AM}} = \sqrt{\frac{2m\mu}{\hbar^2} - (k_y - \alpha_y)^2}, \quad (27)$$

$$k_e^s \approx k_h^s \approx k^s = \sqrt{\frac{2m\mu}{\hbar^2} - k_y^2}, \quad (28)$$

where k_e^s and k_h^s are wavevectors of transmitting wave for SC. The concrete form of k_e^s and k_h^s are given by Eqs. A3 and A4. Then, we obtain the following forms of the conductance in the normal state σ_{ρ}^N and superconducting state σ_{ρ}^S ,

$$\sigma_{\rho}^N(E, k_y) = \frac{\tilde{q}_{\rho}^{\text{AM}} \tilde{k}^s}{Z^2 + \frac{1}{4} (\tilde{q}_{\rho}^{\text{AM}} + \tilde{k}^s)^2} \quad (29)$$

$$r_\rho = \frac{\frac{1}{2}(\tilde{q}_\rho^{\text{AM}} - \tilde{k}^s) + iZ}{\frac{1}{2}(\tilde{q}_\rho^{\text{AM}} + \tilde{k}^s) + iZ} \frac{\Gamma_+\Gamma_-}{1 - [1 - \sigma_\rho^N(E, k_y)]\Gamma_+\Gamma_-} \quad (30)$$

$$r_\rho^A = \begin{cases} \text{sgn}(\rho) \frac{\Gamma_+\sigma_\rho^N(E, k_y)}{1 - [1 - \sigma_\rho^N(E, k_y)]\Gamma_+\Gamma_-} & \text{singlet} \\ \frac{\Gamma_+\sigma_\rho^N(E, k_y)}{1 - [1 - \sigma_\rho^N(E, k_y)]\Gamma_+\Gamma_-} & \text{triplet} \end{cases} \quad (31)$$

$$\frac{\sigma_\rho^S(E, k_y)}{\sigma_\rho^N(E, k_y)} = \frac{1 + \sigma_\rho^N(E, k_y) |\Gamma_+|^2 - [1 - \sigma_\rho^N(E, k_y)] |\Gamma_+\Gamma_-|^2}{|1 - [1 - \sigma_\rho^N(E, k_y)]\Gamma_+\Gamma_-|^2} \quad (32)$$

with $\rho = \uparrow, \downarrow$. In the above, $\tilde{q}_\rho^{\text{AM}}$, \tilde{k}^s , and Γ_\pm are given by

$$\tilde{q}_\rho^{\text{AM}} = \frac{q_\rho^{\text{AM}}}{k_F}, \quad \tilde{k}^s = \frac{k^s}{k_F}, \quad k_F = \frac{\sqrt{2m\mu}}{\hbar}, \quad (33)$$

$$\Gamma_+ = \frac{\Delta^*(\theta_+)}{E + \Omega_+}, \quad \Gamma_- = \frac{\Delta(\theta_-)}{E + \Omega_-}, \quad (34)$$

$$\theta_+ = \arcsin \frac{k_y}{k_F}, \quad \theta_- = \pi - \theta_+, \quad (35)$$

$$\Omega_\pm = \lim_{\delta \rightarrow 0_+} \sqrt{(E + i\delta)^2 - |\Delta(\theta_\pm)|^2}. \quad (36)$$

It is noted that Eq. (32) has the same structure as compared to the tunneling conductance formula in normal metal / unconventional superconductor junctions³⁵. Here, the values with a tilde represent that they are divided by the Fermi wavenumber in SC and Z is the dimensionless parameter

$$Z = \frac{mU}{\hbar^2 k_F} \quad (37)$$

If we consider spin-triplet superconductors with arbitrary direction of \mathbf{d} -vector, the pair potential can be written as

$$\hat{\Delta}(\pm \hat{\mathbf{k}}) = \pm i \mathbf{d}(\theta) \cdot \hat{\boldsymbol{\sigma}} \hat{\sigma}_y = \pm \begin{bmatrix} -d_x(\theta) + id_y(\theta) & d_z(\theta) \\ d_z(\theta) & d_x(\theta) + id_y(\theta) \end{bmatrix}, \quad (38)$$

with Pauli matrices

$$\hat{\boldsymbol{\sigma}} = (\hat{\sigma}_x, \hat{\sigma}_y, \hat{\sigma}_z), \quad (39)$$

$$\hat{\sigma}_x = \begin{bmatrix} 0 & 1 \\ 1 & 0 \end{bmatrix}, \quad \hat{\sigma}_y = \begin{bmatrix} 0 & -i \\ i & 0 \end{bmatrix}, \quad \hat{\sigma}_z = \begin{bmatrix} 1 & 0 \\ 0 & -1 \end{bmatrix}. \quad (40)$$

In addition to the $\mathbf{d} \parallel \hat{\mathbf{z}}$ case, we perform calculations for $\mathbf{d} \parallel \hat{\mathbf{x}}$ case, where the pair potential can be written as

$$\pm \hat{\Delta}(\pm \hat{\mathbf{k}}) = \begin{bmatrix} -\Delta(\theta) & 0 \\ 0 & \Delta(\theta) \end{bmatrix} \quad (41)$$

with $\hat{\mathbf{x}}$ and $\hat{\mathbf{z}}$ being the unit vectors parallel to the x -axis and the z -axis, respectively.

In the presence of a magnetically active barrier, the barrier potential should be expressed by 2×2 matrix with

$$\hat{Z} = \text{diag}(Z_{\uparrow}, Z_{\downarrow}) = \frac{m\hat{U}_0}{\hbar k_F^2}. \quad (42)$$

For a spin- \uparrow (\downarrow) electron with a particular value of k_y contributing to the conduction process, the incident electron and the transparent electron must form traveling waves. For $|E|, |\Delta(\theta_{\pm})| \ll \mu$, this condition can be approximately rewritten as

$$k_{\uparrow(\downarrow)}^{\min} < k_y < k_{\uparrow(\downarrow)}^{\max}, \quad (43)$$

where

$$k_{\uparrow}^{\min} = \max(-k_F, -k_F - \alpha_y), k_{\uparrow}^{\max} = \min(k_F, k_F - \alpha_y), \quad (44)$$

$$k_{\downarrow}^{\min} = \max(-k_F, -k_F + \alpha_y), k_{\downarrow}^{\max} = \min(k_F, k_F + \alpha_y), \quad (45)$$

as we can see in Fig. 2. Especially for $|E| < |\Delta(\theta_{\pm})|$, Andreev reflection is needed for the conduction process. In the cases of spin-singlet pairing or spin-triplet pairing with $\mathbf{d} \parallel \hat{\mathbf{z}}$, the spin- \uparrow (\downarrow) electron is reflected as a spin- \downarrow (\uparrow) hole. The wave vector of the reflected hole is nearly equivalent to that of a spin- \uparrow (\downarrow) electron for $|E|, |\Delta(\theta_{\pm})| \ll \mu$. Hence, the condition Eq. (43) does not change. On the other hand, in the case of spin-triplet pairing with $\mathbf{d} \parallel \hat{\mathbf{x}}$, the spin- \uparrow (\downarrow) electron is reflected as a spin- \uparrow (\downarrow) hole. The wave vector of the reflected hole is nearly equivalent to that of a spin- \downarrow (\uparrow) electron for $|E|, |\Delta(\theta_{\pm})| \ll \mu$. This changes the condition Eq. (43) for $|E|, |\Delta(\theta_{\pm})| \ll \mu$ into

$$k^{\min} < k_y < k^{\max} \quad (46)$$

for both spin- \uparrow and spin- \downarrow electrons, where

$$k^{\min} = -k_F + |\alpha_y|, k^{\max} = k_F - |\alpha_y|. \quad (47)$$

It is noted that the strength of AM must satisfy $|\alpha_y|/k_F < 2$ to satisfy $k_{\uparrow(\downarrow)}^{\min} < k_{\uparrow(\downarrow)}^{\max}$ in Eq. (43).

III. RESULTS

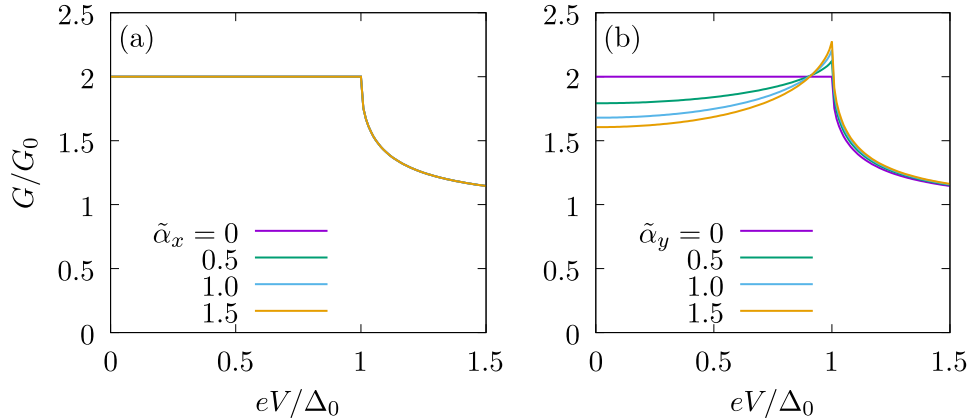


FIG. 4. Normalized conductance G/G_0 of p -wave altermagnet /insulator/superconductor junctions with s -wave superconductor without the barrier potential ($Z = 0$) for (a) p_x -wave altermagnet case where the Fermi surfaces shifts to the x -direction, and for (b) p_y -wave altermagnet case where the Fermi surfaces shift to the y -direction.

In Fig. 4, the normalized conductance of AM/I/SC junction G/G_0 as a function of the bias voltage V is plotted for various values of $\tilde{\alpha} = (\tilde{\alpha}_x, \tilde{\alpha}_y) = \alpha/k_F$. Here, we choose conventional s -wave superconductor where pair potential is given by Δ_0 . Figure 4(a) shows the results for p_x -wave AM with α parallel to the x -axis, *i.e.*, the normal to the interface. It is noted that G does not depend on $\tilde{\alpha}_x$ as shown in Fig. 4(a) since $\tilde{q}_\rho^{\text{AM}}$ is independent of $\tilde{\alpha}_x$. On the other hand, as shown in Fig. 4(b), G depends on $\tilde{\alpha}_y$ since $\tilde{q}_\rho^{\text{AM}}$ depends on $\tilde{\alpha}_y$. It is noted that when we change the sign of the bias voltage V , G/G_0 always becomes an even function of eV for the results in this paper.

In Fig. 5, the normalized conductance of AM/I/SC junction G/G_0 as a function of $\tilde{\alpha}_x$ is plotted with a fixed value of $\tilde{\alpha}_y$ for various values of $E = eV$. This shows that the conductance does not change by $\tilde{\alpha}_x$ even for $\tilde{\alpha}_y \neq 0$ as proved generally by Eqs. (11), (12), and (B1)–(B4). Thus we can assume $\tilde{\alpha}_x = 0$ without loss of generality. In the rest of this chapter, we show the results for p_y -wave AM cases with $\alpha \parallel \hat{y}$.

Figures 6–10 show the $\tilde{\alpha}_y$ dependence of G/G_0 for various types of pairing symmetry of SC. As shown in Figs. 6(a), (b), (d), and (e) for s -wave SC with $\Delta(\theta) = \Delta_0$ and $d_{x^2-y^2}$ -wave SC with anisotropic pair potential $\Delta(\theta) = \Delta_0 \cos 2\theta$, normalized conductance G/G_0 is suppressed with the increase of $|\tilde{\alpha}_y|$ around zero bias voltage either in high-transparency ($Z = 0$)

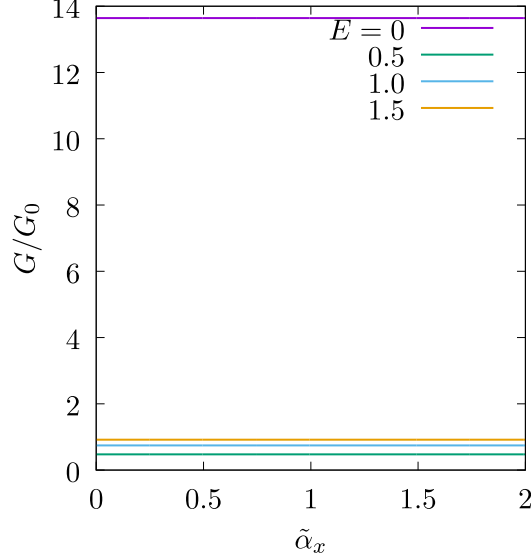


FIG. 5. Normalized conductance G/G_0 of p -wave altermagnet/insulator/ d_{xy} -wave superconductor junction. The barrier potential is set to $Z = 2$ and $\tilde{\alpha}_y$ is fixed to $\tilde{\alpha}_y = 0.5$.

or low-transparency junction ($Z = 2$). This result can be understood by the suppression of the magnitude of $\sigma_{\uparrow(\downarrow)}^N(E, k_y)$. The discrepancy between two values of $\tilde{q}_{\uparrow(\downarrow)}^{AM}$ and \tilde{k}^S makes $\sigma_{\uparrow(\downarrow)}^N(E, k_y)$ in Eq. (29) smaller. This yields a smaller value of $\sigma_{\uparrow(\downarrow)}^S(E, k_y)/\sigma_{\uparrow(\downarrow)}^N(E, k_y)$ for s - and $d_{x^2-y^2}$ -wave SC where $|\Gamma_+| = |\Gamma_-| = 1, \Gamma_+\Gamma_- = -1$ are satisfied for any k_y at $E = 0$. In contrast, Figs. 6(c) and (f) show that, for d_{xy} -wave SC with $\Delta(\theta) = \Delta_0 \sin 2\theta$, G/G_0 is enhanced with the increase of $|\tilde{\alpha}_y|$ for almost all of $|\tilde{\alpha}_y|$ with $0 \leq |\tilde{\alpha}_y| \leq 2$. It can be understood that the decrease of $\sigma_{\uparrow(\downarrow)}^N(E, k_y)$ results in larger magnitude of $\sigma_{\uparrow(\downarrow)}^S(E, k_y)/\sigma_{\uparrow(\downarrow)}^N(E, k_y)$ for d_{xy} -wave SC where $|\Gamma_+| = |\Gamma_-| = 1, \Gamma_+\Gamma_- = 1$ are satisfied for any k_y at $E = 0$.

It is noted that Eq. (32) shows that $\sigma_{\uparrow(\downarrow)}^S(E, k_y) = 2$ is always satisfied for d_{xy} -wave SC case regardless of the values of Z and $\tilde{\alpha}_y$. This means that an electron at $E = 0$ injected from the AM side is reflected as a hole by Andreev reflection with probability unity no matter how strong the barrier potential of the insulator is. This is because the group velocities of an incident electron and the corresponding Andreev-reflected hole are the same value in the limit of $|E|/\mu \ll 1$ in the case of p -wave AM/I/SC junction, whereas they differ in the case of d -wave AM/I/SC junction for the general k_y ¹⁷.

We perform a similar calculation for spin-triplet SCs as shown in Fig. 7. Figures 7(a), (b), (e), and (f) show that in the cases with $\mathbf{d} \parallel \hat{\mathbf{z}}$, G/G_0 is enhanced with the increase of $|\tilde{\alpha}_y|$ around the zero bias voltage for p_x -wave SC with $\Delta(\theta) = \Delta_0 \cos \theta$, while G/G_0

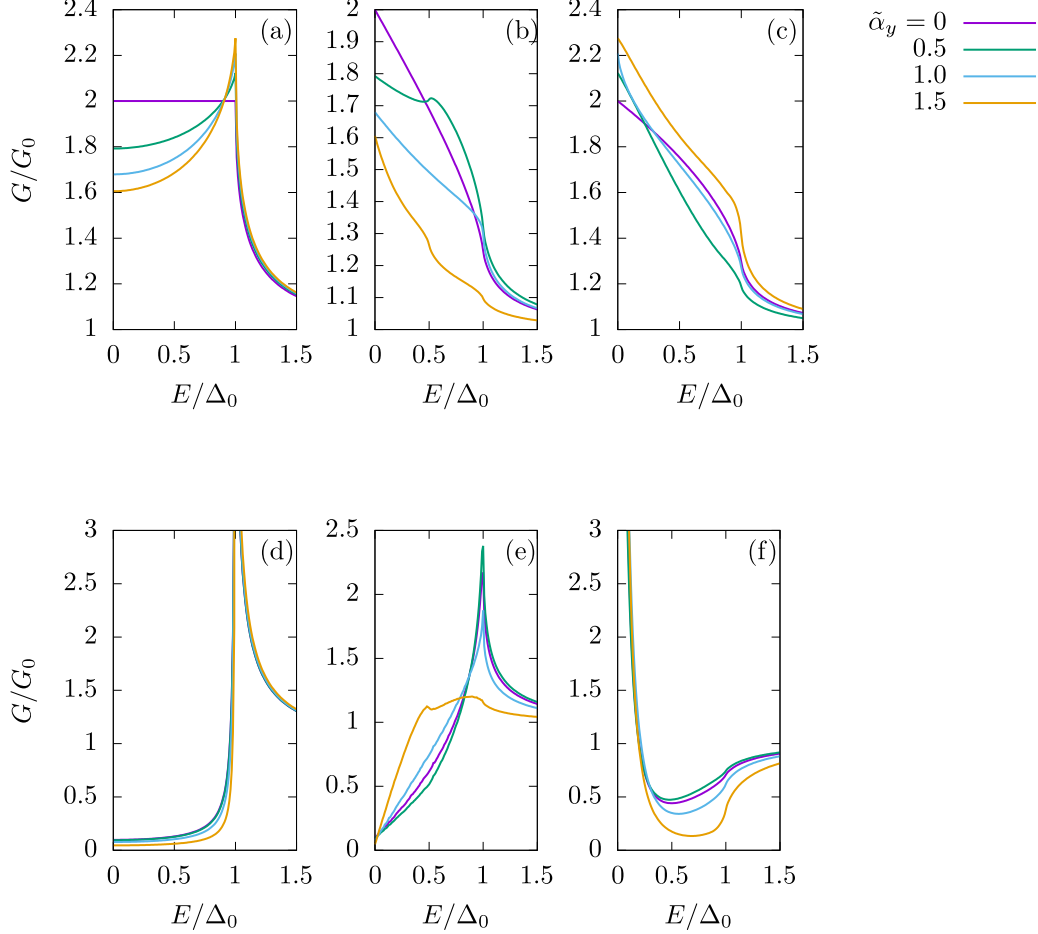


FIG. 6. Normalized conductance G/G_0 of p_y -wave altermagnet/insulator/superconductor junctions with spin-singlet superconductors. The barrier potential $Z = 0$ for upper panels ((a),(b),(c)), and $Z = 2$ for lower panels ((d),(e),(f)). The pairing symmetry of SCs are s -wave ((a),(d)), $d_{x^2-y^2}$ -wave SC((b),(e)), and d_{xy} -wave((c),(f)).

is suppressed with the increase of $|\tilde{\alpha}_y|$ around the zero bias voltage for p_y -wave SC with $\Delta(\theta) = \Delta_0 \sin \theta$. These features are consistent with Eqs. (29)-(32) again, which is available for both spin-singlet SC and spin-triplet SC with $\mathbf{d} \parallel \hat{z}$.

By contrast, for $\mathbf{d} \parallel \hat{x}$, as shown in Figs. 7(c), (d), (g), and (h), G/G_0 is strongly suppressed by $|\tilde{\alpha}_y|$. Especially, the conductance becomes 0 at $eV = 0$ for $|\tilde{\alpha}_y| \geq 1$. This result can be explained as follows. For $\mathbf{d} \parallel \hat{x}$, an injected electron and the Andreev-reflected hole must have the same spin angular momentum. Andreev reflection only occurs for k_y with which both $k_{e\uparrow(\downarrow)}^+$ and $k_{h\uparrow(\downarrow)}^-$ are real numbers. As shown in Eqs. (15) and (17) ((16) and (18)), the region of k_y where both $k_{e\uparrow(\downarrow)}^+$ and $k_{h\uparrow(\downarrow)}^-$ are real becomes narrow with the

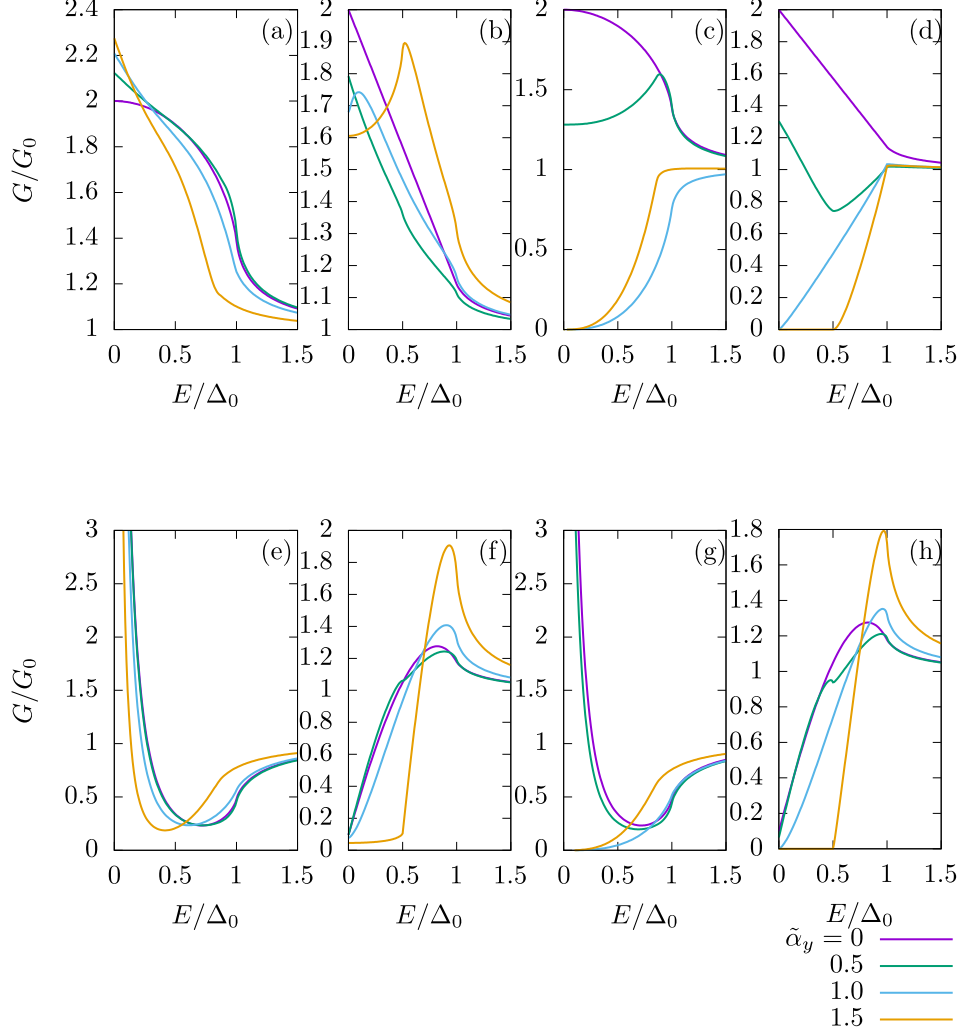


FIG. 7. Normalized conductance G/G_0 of p_y -wave altermagnet/insulator/superconductor junctions with spin-triplet superconductors. The barrier potential $Z = 0$ for upper panels ((a), (b), (c), (d)), and $Z = 2$ for lower panels ((e), (f), (g), (h)). The pairing symmetry of SCs are p_x -wave ((a),(e)), p_y -wave ((b),(f)) with $\mathbf{d} \parallel \hat{\mathbf{z}}$, and p_x -wave ((c),(g)), p_y -wave ((d),(h)) with $\mathbf{d} \parallel \hat{\mathbf{x}}$.

increase of $|\tilde{\alpha}_y|$. This results in a more strict condition for k_y to make conduction possible than that in the normal metal case. Especially, for $|\tilde{\alpha}_y| \geq 1$, at least one of $k_{e\uparrow(\downarrow)}^+$ and $k_{h\uparrow(\downarrow)}^-$ becomes imaginary number for all of k_y with $|eV| \ll \mu$, which results in $G/G_0 = 0$.

To summarize the results so far, we calculate G/G_0 at $eV = 0$ as a function of $\tilde{\alpha}_y$ as shown in Figs. 8 and 9. These figures show that the zero-bias conductance of p_y -wave AM/I/SC junction is dramatically changed by the pairing symmetry of the superconductor and that the junction can be used to detect the pairing symmetry. We also anticipate

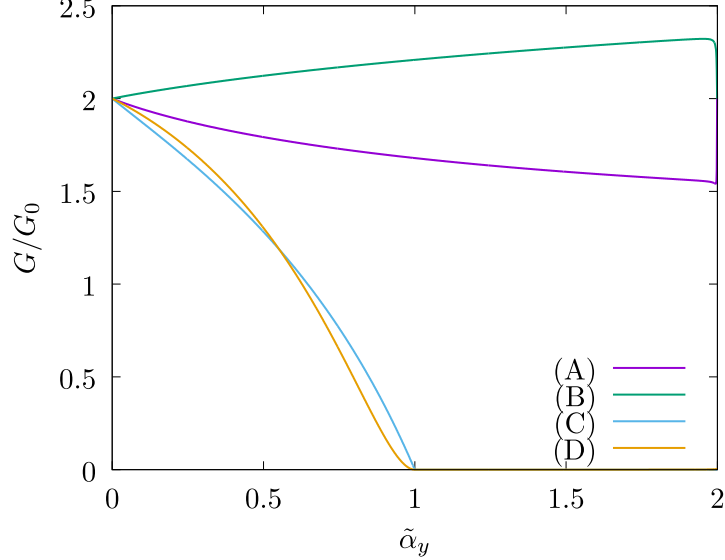


FIG. 8. The $\tilde{\alpha}_y$ dependence of zero bias conductance at $Z = 0$. Pairing symmetries of SCs are (A) s -wave, p_y -wave with $\mathbf{d} \parallel \hat{z}$, $d_{x^2-y^2}$ -wave, (B) p_x -wave with $\mathbf{d} \parallel \hat{z}$, d_{xy} -wave, (C) p_x -wave with $\mathbf{d} \parallel \hat{x}$, and (D) p_y -wave with $\mathbf{d} \parallel \hat{x}$

that it is possible to determine the symmetries of unknown candidates of AM by measuring the zero-bias conductance of AM/SC junctions. Actually, Figs. 8 and 9 show that the conductance of the p -wave AM/spin-triplet SC junction with $\mathbf{d} \parallel \hat{z}$ is generally larger than that of the cases with the $\mathbf{d} \perp \hat{z}$. On the other hand, Figs. 18 and 19 in Appendix C show that the conductance for the $\mathbf{d} \parallel \hat{z}$ case is smaller than or equal to that for the $\mathbf{d} \perp \hat{z}$ case. Qualitative change of unnormalized zero-bias conductance is summarized in Table I. The most significant difference between the cases of a p -wave AM junction and a d -wave AM one is that the change of conductance under the $\pi/2$ rotation of the c -crystal axis. In the case of a p -wave AM junction, the normalized exchange energy ($\tilde{\alpha}_x$ or $\tilde{\alpha}_y$) dependence of the conductance significantly changes because of the broken fourfold symmetry of the Fermi surface, while there is no change in the case of a d -wave AM junction. In addition, the suppression of the conductance by the exchange energy of the d -wave AM junction is relatively smaller than that of the p -wave cases for $\mathbf{d} \perp \hat{z}$.

As shown in Fig. 10, the $\tilde{\alpha}_y$ dependence of G/G_0 becomes more complicated for chiral p -wave SC with the pair potential $\Delta(\theta) = \Delta_0 e^{i\theta}$ and chiral d -wave one with $\Delta(\theta) = \Delta_0 e^{2i\theta}$ as compared to Figs. 6 and 7.

To clarify these features, we calculate G/G_0 for chiral SC cases at $eV = 0$ as a function

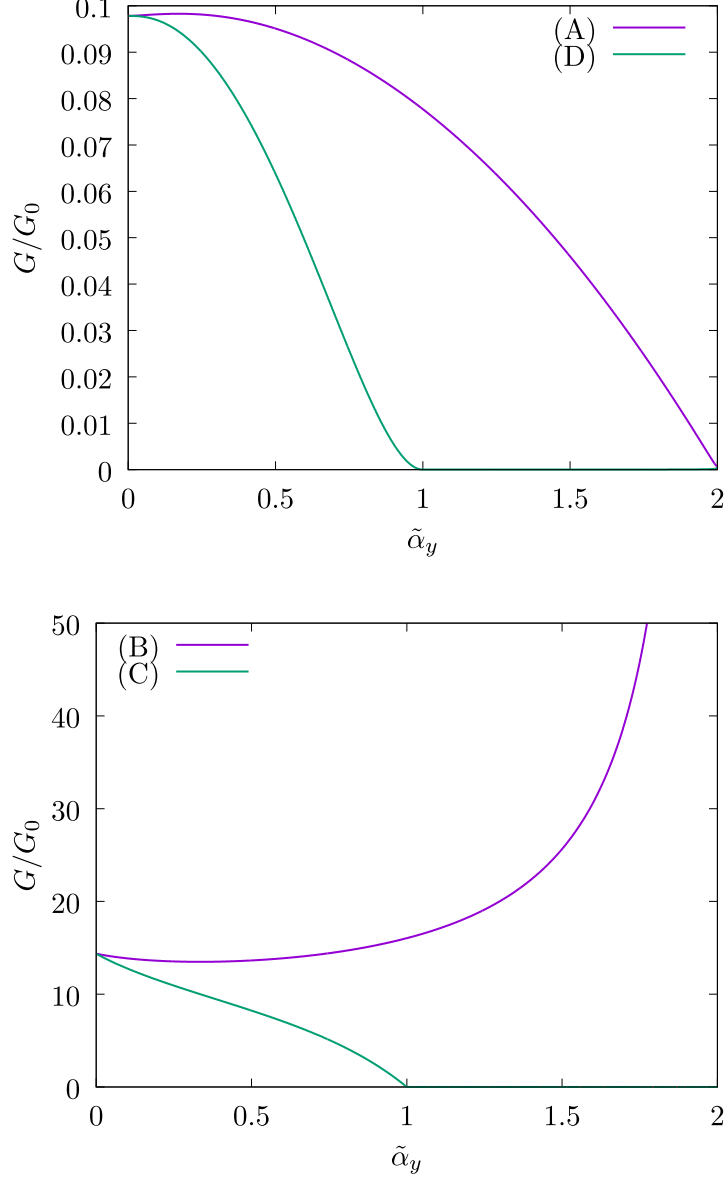


FIG. 9. The $\tilde{\alpha}_y$ dependence of zero bias conductance at $Z = 2$. The pairing symmetry of SCs are (A) s -wave, p_y -wave with $\mathbf{d} \parallel \hat{z}$, $d_{x^2-y^2}$ -wave, (B) p_x -wave with $\mathbf{d} \parallel \hat{z}$, d_{xy} -wave, (C) p_x -wave with $\mathbf{d} \parallel \hat{x}$, and (D) p_y -wave with $\mathbf{d} \parallel \hat{x}$

of $\tilde{\alpha}_y$ as shown in the left panels of Figs. 11 and 12. G/G_0 has at most one local maximum in the chiral p -wave SC cases, while for chiral d -wave SC, G/G_0 has two local maxima, as shown in Figs. 11 and 12. These features are significantly different from those of p_x -wave and d_{xy} -wave pairings. For the comparison, we show the value of G and G_0 for chiral SC cases at $eV = 0$ as a function of $\tilde{\alpha}_y$ divided by each maximum value \tilde{G} or \tilde{G}_0 in the right panels of Figs. 11 and 12. Since both G and G_0 are monotonic decreasing functions of $|\tilde{\alpha}_y|$

TABLE I. The qualitative change of conductance G of AM/I/SC junctions with the increase of the normalized strength of altermagnets $\tilde{\alpha}_x, \tilde{\alpha}_y, \tilde{\alpha}_1$, or $\tilde{\alpha}_2$ where $\tilde{\alpha}_x$ and $\tilde{\alpha}_y$ denote the normalized strength of the exchange field in p -wave altermagnet and $\tilde{\alpha}_1$ and $\tilde{\alpha}_2$ denote those in d -wave altermagnet. It is noted that the values of conductance are not normalized by that in the normal state. These results occur for both the cases $Z = 2$ and $Z = 5$. The expressions “decrease*” and “decrease**” indicate that the conductance reaches 0 when the strength of AMs $\tilde{\alpha}_x, \tilde{\alpha}_y, \tilde{\alpha}_1$, or $\tilde{\alpha}_2$ reaches 1 and 2, respectively. On the other hand, “suppressed” and “enhanced” denote that the change of the conductance is insignificant.

	p_x AM	p_y AM	d_{xy} AM	$d_{x^2-y^2}$ AM
p_x SC $\mathbf{d} \parallel \hat{z}$	constant	decrease**	constant	decrease*
p_x SC $\mathbf{d} \perp \hat{z}$	constant	decrease*	constant	suppressed
chiral- p SC $\mathbf{d} \parallel \hat{z}$	constant	decrease**	enhanced	decrease*
chiral- p SC $\mathbf{d} \perp \hat{z}$	constant	decrease*	enhanced	suppressed

and $\partial G_0/\partial \tilde{\alpha}_y$ does not vary significantly by $\tilde{\alpha}_y$, G/G_0 is enhanced with the increase of $\tilde{\alpha}_y$ when $|\partial G/\partial \tilde{\alpha}_y|$ has a particularly small value.

To understand this non-monotonic $\tilde{\alpha}_y$ dependence of G/G_0 for chiral SC cases, we show the k_y - and spin-resolved conductance of AM/I/SC junction $\sigma_{\uparrow}^S(E, k_y)$ and $\sigma_{\downarrow}^S(E, k_y)$ in Figs. 13–15. As shown in Figs. 15(a), (d), 14(a), (d), and 13(a), (d), the energy dispersion corresponding to the maximum value of $\sigma_{\uparrow}^S(E, k_y)$ and $\sigma_{\downarrow}^S(E, k_y)$ at $\tilde{\alpha}_y = 0$ corresponds to so-called chiral edge mode. As the value of $|\tilde{\alpha}_y|$ increases, the range of k_y contributing to the conduction process becomes restricted.

Both in the cases of the spin-triplet chiral p -wave SC with $\mathbf{d} \parallel \hat{z}$ and spin-singlet chiral d -wave SC, the range of k_y contributing to the conduction process becomes restricted as shown in Figs. 13 and 14. This corresponds to Eq. (43). For the other values, $\sigma_{\uparrow(\downarrow)}^S(E, k_y) = 0$.

For generality, we assume $\sigma_{\uparrow(\downarrow)}^S(E = 0, k_y)$ is prominently enhanced around $k_y = \pm k_1, \pm k_2, \dots, \pm k_M$ with $0 \leq k_1 < k_2 < \dots < k_M$ corresponding to chiral edge mode with $E = 0$ in spin-singlet SC or spin-triplet SC with $\mathbf{d} \parallel \hat{x}$. Here, the integer M is related to the

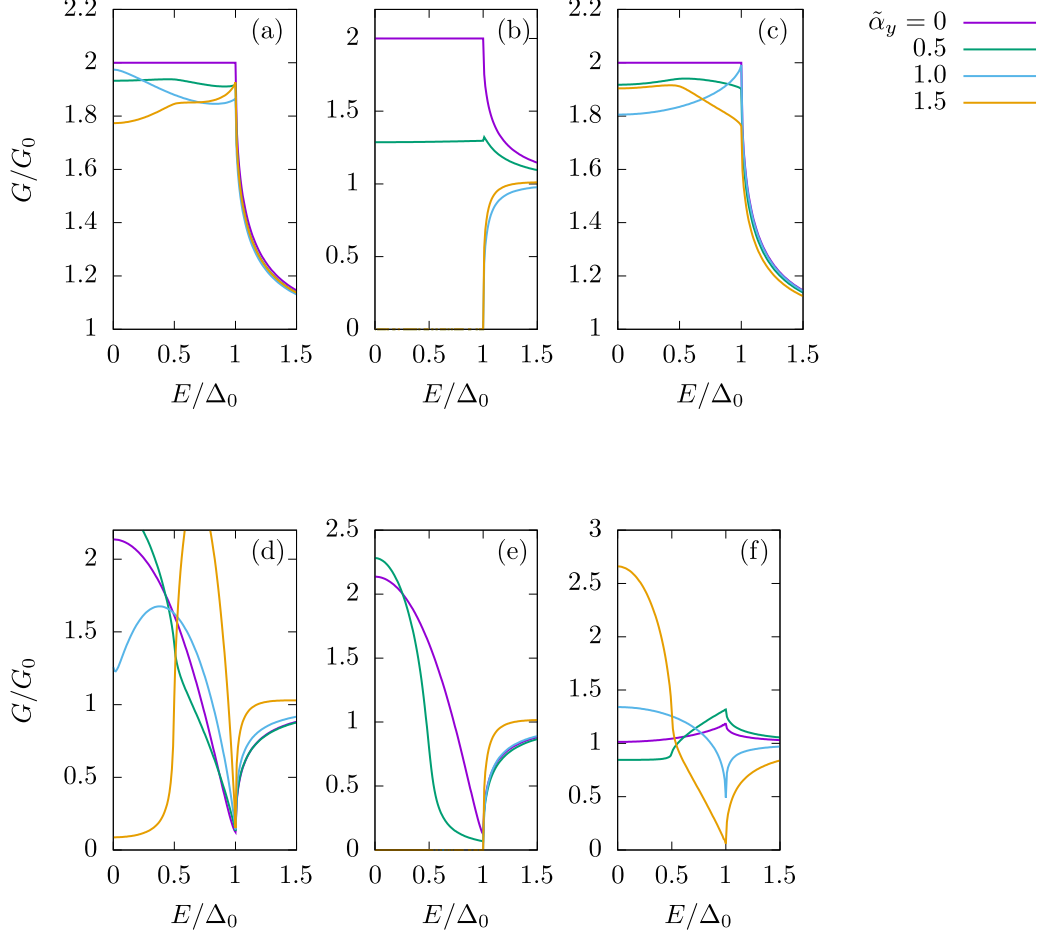


FIG. 10. Normalized conductance G/G_0 of p_y -wave altermagnet/insulator/superconductor junctions with chiral superconductors. The barrier potential $Z = 0$ for upper panels ((a), (b), (c)), and $Z = 2$ for lower panels ((d), (e), (f)). The pairing symmetry of SCs are chiral p -wave with $\mathbf{d} \parallel \hat{z}$ ((a), (d)), chiral p -wave SC with $\mathbf{d} \parallel \hat{x}$ ((b), (e)), and chiral d -wave ((c), (f)).

number of chiral-edge modes N as

$$\begin{cases} M = \frac{N+1}{2}, k_1 = 0 & \text{for odd } N, \\ M = \frac{N}{2}, k_1 \neq 0 & \text{for even } N. \end{cases} \quad (48)$$

When $|\tilde{\alpha}_y| < 1 \pm k_M/k_F$ is satisfied, except for $|\tilde{\alpha}_y| \approx 1 \pm k_i/k_F$ with $i = 1, 2, \dots, M$, the increase of $|\tilde{\alpha}_y|$ does not substantially influence G at $E = 0$ since the values of $\sigma_{\uparrow(\downarrow)}^S(E = 0, k_y)$ at $k_{\uparrow(\downarrow)}^{\min}, k_{\uparrow(\downarrow)}^{\max}$ are much smaller than that for $k_y \approx \pm k_1, \pm k_2, \dots, \pm k_M$. On the other hand, for $|\tilde{\alpha}_y| \approx 1 \pm k_i/k_F$ with $i = 1, 2, \dots, M$, the increase of $|\tilde{\alpha}_y|$ significantly suppresses G at $E = 0$ since $|k_{\uparrow}^{\max}| = |k_{\downarrow}^{\min}| \approx k_i$ ($|k_{\downarrow}^{\max}| = |k_{\uparrow}^{\min}| \approx k_i$) and the values of $\sigma_{\uparrow(\downarrow)}^S(E = 0, k_y)$ at k_{\uparrow}^{\max} and k_{\downarrow}^{\min} (k_{\downarrow}^{\max} and k_{\uparrow}^{\min}) are not significantly smaller than the maximum value

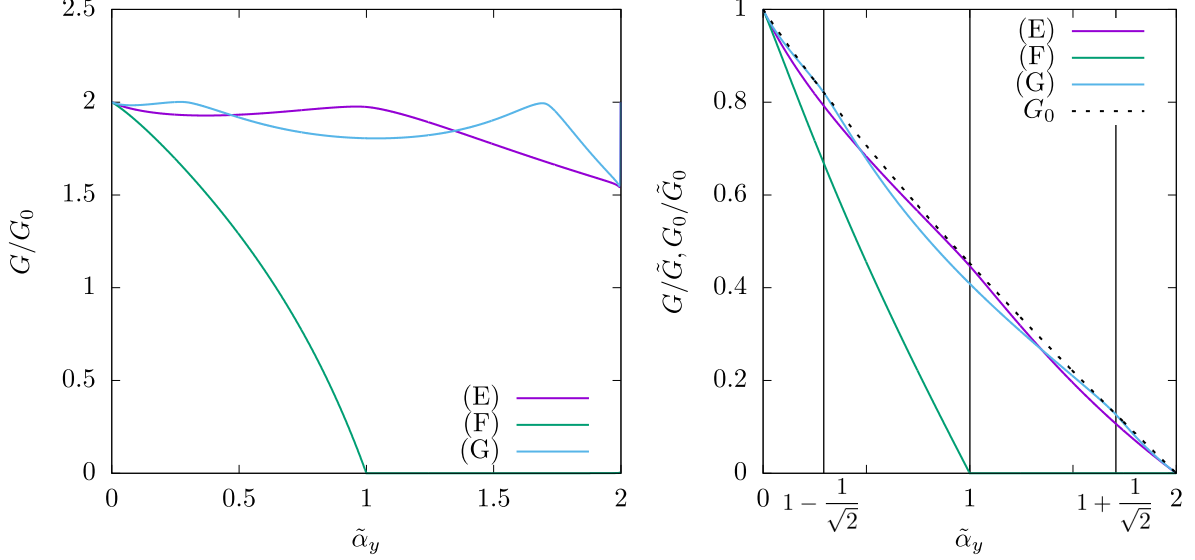


FIG. 11. The $\tilde{\alpha}_y$ dependence of normalized zero-bias conductance G/G_0 (left panel) and the unnormalized value G divided by its maximum value \tilde{G} (right panel) at $Z = 0$. Pairing symmetries of SCs are (E)chiral p -wave with $\mathbf{d} \parallel \hat{z}$, (F)chiral p -wave with $\mathbf{d} \parallel \hat{x}$, and (G)chiral d -wave. The dotted line corresponds to the conductance of the normal-metal state G_0 .

of $\sigma_{\uparrow(\downarrow)}^S(E = 0, k_y)$. When the value of $|\tilde{\alpha}_y|$ exceeds $1 + k_M/k_F$, the maximum value of $\sigma_{\uparrow(\downarrow)}^S(E = 0, k_y)$ for Eq. (43) is reduced and G/G_0 is suppressed with the increase of $|\tilde{\alpha}_y|$. Hence, G/G_0 at $E = 0$ as a function of $|\tilde{\alpha}_y|$ has N local maxima. As shown in Fig. 13, $\sigma_{\uparrow(\downarrow)}^S(E = 0, k_y)$ is prominently enhanced around $k_y = 0$ for chiral p -wave SC with $\mathbf{d} \parallel \hat{z}$. This corresponds to $N = 1$ and G/G_0 at $E = 0$ as a function of $|\tilde{\alpha}_y|$ has one local maximum. Since $N = 2$ (in the present calculation, $k_1/k_F = 1/\sqrt{2}$) for chiral d -wave SC as shown in Fig. 14, the corresponding G/G_0 at $E = 0$ as a function of $|\tilde{\alpha}_y|$ has two local maxima.

In the case of the spin-triplet chiral p -wave SC with $\mathbf{d} \parallel \hat{x}$, the range of k_y contributing to the conduction process becomes restricted as shown in Fig. 15. This corresponds to Eq. (46). For the other values, $\sigma_{\uparrow(\downarrow)}^S(E, k_y) = 0$ with $|E| < \Delta_0$. As we see in Fig. 15, $\sigma_{\uparrow(\downarrow)}^S(E = 0, k_y)$ is prominently enhanced around $k_y = 0$ for the chiral p -wave pairing case with $\mathbf{d} \parallel \hat{x}$. For sufficiently large Z with strong barrier, when $|\tilde{\alpha}_y| < 1$ is satisfied, except for $|\tilde{\alpha}_y| \approx 1$, the increase of $|\tilde{\alpha}_y|$ does not substantially influence G at $E = 0$ since the values of $\sigma_{\uparrow(\downarrow)}^S(E = 0, k_y)$ at $k_y = k^{\min}$ and $k_y = k^{\max}$ are much smaller than that for $k_y \approx 0$. However, for $|\tilde{\alpha}_y| \approx 1$, the increase of $|\tilde{\alpha}_y|$ significantly suppresses G at $E = 0$. In this case, $|k^{\min}| = |k^{\max}| \approx 0$ is satisfied, and the values of $\sigma_{\uparrow(\downarrow)}^S(E = 0, k_y \neq 0)$ at k^{\min} and k^{\max}

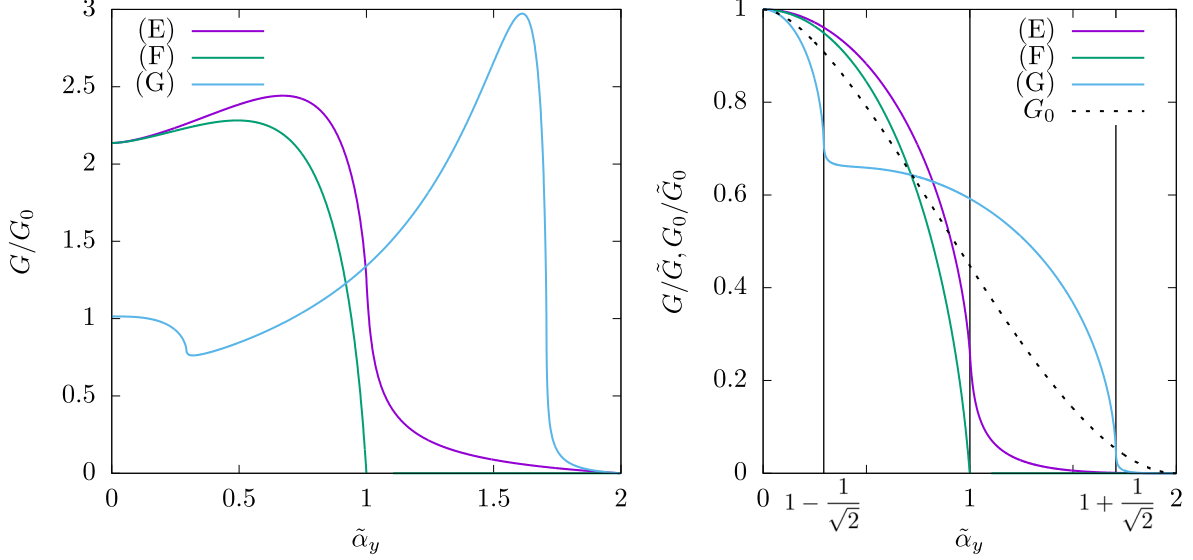


FIG. 12. The $\tilde{\alpha}_y$ dependence of normalized zero-bias conductance G/G_0 (left panel) and the unnormalized value G divided by its maximum value \tilde{G} (right panel) at $Z = 2$. Pairing symmetries of SCs are (E)chiral p -wave with $\mathbf{d} \parallel \hat{z}$, (F)chiral p -wave with $\mathbf{d} \parallel \hat{x}$, and (G)chiral d -wave. The dotted line corresponds to the conductance of the normal-metal state G_0 .

are not significantly smaller as compared to the maximum value $\sigma_{\uparrow(\downarrow)}^S(E = 0, k_y = 0)$. This results in suppression of G/G_0 like the other spin-triplet SC cases shown in Figs. 7(c), (d), (g), and (h). It is noted that, for a weak barrier, $\sigma_{\uparrow(\downarrow)}^S(E = 0, k_y)$ at k_y apart from $k_y \approx 0$ is a little bit smaller than $\sigma_{\uparrow(\downarrow)}^S(E = 0, k_y = 0)$, and G decreases almost linearly as a function of $|\tilde{\alpha}_y|$ for $|\tilde{\alpha}_y| < 1$ as shown in the right panel of Fig. 11. This may lead to no local maxima of G/G_0 as shown in Fig. 11(G).

It is noted that the non-monotonic changes of G/G_0 as a function of the strength of AM in AM / I / chiral SC junction like those shown in Figs. 11 and 12 cannot be seen in the d -wave AM case as shown in Appendix C.

Since electrons in AM are spin-polarized in each sublattice like those in conventional antiferromagnet², p -wave AM strictly leads to time-reversal symmetry breaking which is not reflected in the Hamiltonian as shown in Eq. (2). The consequence of antiferromagnetic spin structure in real space may appear in the boundary condition of each spin. Since the distances of the sublattice from the boundary for \uparrow and \downarrow spin are different from each other, the boundary condition or the barrier potential is spin-dependent. To estimate the effect of this, we perform the calculation of the normalized conductance G/G_0 as a function of

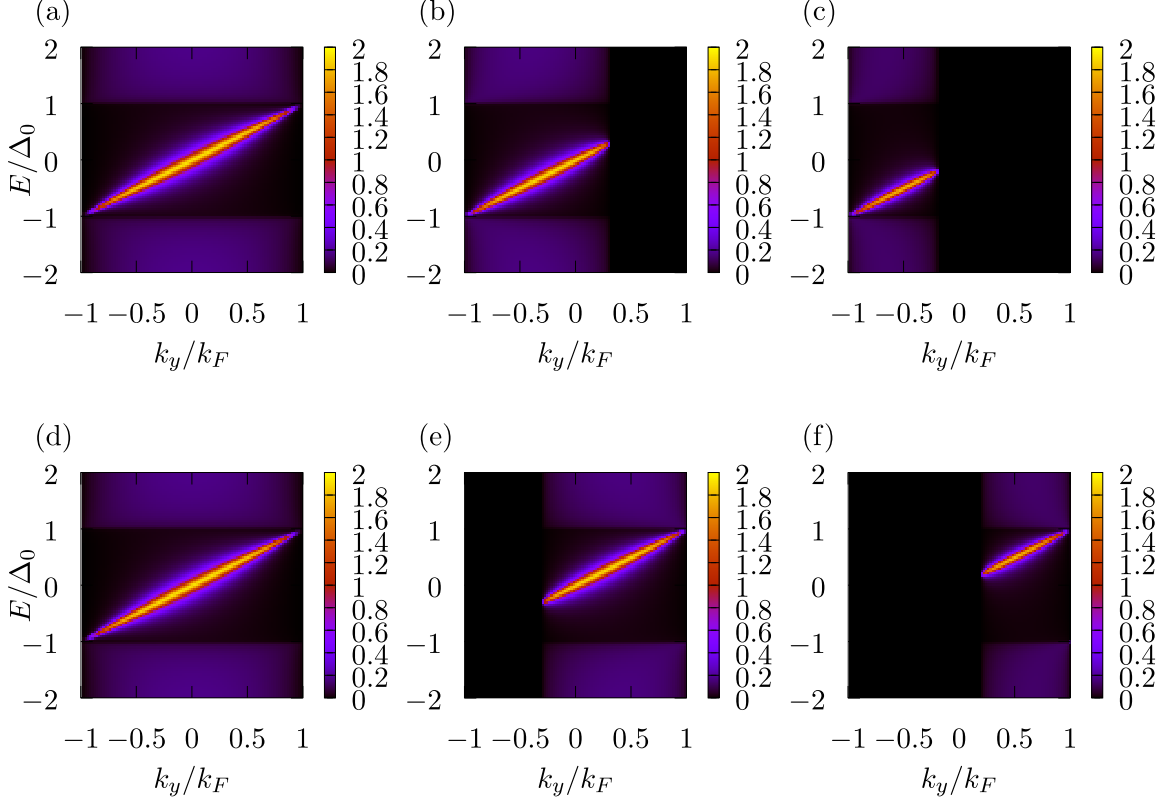


FIG. 13. Momentum resolved conductance $\sigma_{\uparrow}^S(E, k_y)$ ((a),(b),(c)) and $\sigma_{\downarrow}^S(E, k_y)$ ((d),(e),(f)) for p_y -wave altermagnet/Insulator/chiral p -wave superconductor with $d \parallel \hat{z}$ junction where $Z = 2$. The strength of p -wave altermagnet is set to $\tilde{\alpha}_y = 0$ ((a),(d)), 0.7 ((b),(e)), and 1.2 ((c),(f)). The number of chiral-edge mode is $N = 1$ and the values of M and k_1 in Eq. (48) becomes $M = 1$ and $k_1/k_F = 0$.

eV with $Z_{\uparrow} \neq Z_{\downarrow}$. For the d_{xy} -wave SC case with $Z_{\uparrow} = Z_{\downarrow}$, the ZBCP appears as shown in Fig. 6(f). When we consider the case with $Z_{\uparrow} \neq Z_{\downarrow}$, the ZBCP splits into two as shown in Fig. 16(a) similar to the case of normal metal / ferromagnetic insulator / d_{xy} -wave superconductor junctions⁵⁸. Fig. 16(b) and (c) show The $\tilde{\alpha}_y$ dependence of zero-bias conductance similar to that for $Z_{\uparrow} = Z_{\downarrow} = 2$. For the d_{xy} -wave pairing, SC is protected by time-reversal symmetry. In this case, our calculating model of the AM/I/SC junction breaks time-reversal symmetry only if $Z_{\uparrow} \neq Z_{\downarrow}$. This results in a qualitative change of conductance by assuming the spin-dependent barrier at the interface. By contrast, conductance changes only quantitatively by assuming the spin-dependent barrier $Z_{\uparrow} \neq Z_{\downarrow}$ at the interface for the chiral p - and chiral d -wave pairing. It is relevant to the fact that the time-reversal symmetry is broken in these superconducting states themselves. We also calculate G/G_0 at $eV = 0$ as

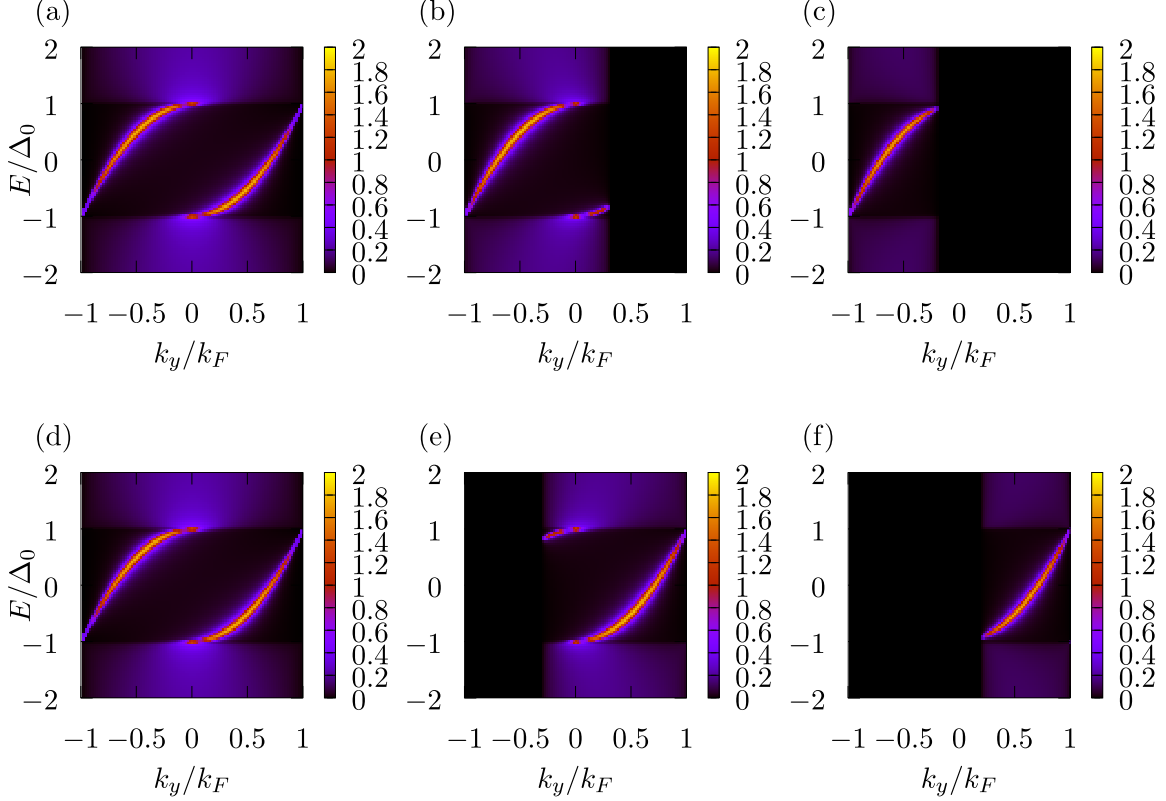


FIG. 14. Momentum resolved conductance $\sigma_{\uparrow}^S(E, k_y)$ ((a),(b),(c)) and $\sigma_{\downarrow}^S(E, k_y)$ ((d),(e),(f)) for p_y -wave altermagnet/Insulator/chiral d -wave superconductor junction where $Z = 2$. The strength of p -wave altermagnet is set to $\tilde{\alpha}_y = 0$ ((a),(d)), 0.7 ((b),(e)), and 1.2 ((c),(f)). The number of chiral-edge modes is $N = 2$ and the values of M and k_1 in Eq. (48) becomes $M = 1$ and $k_1/k_F = 1/\sqrt{2}$.

a function of $\tilde{\alpha}_y$ with $Z_{\uparrow} \neq Z_{\downarrow}$ as shown in Fig. 17. In this figure, we see one local maximum for chiral p -wave SC and two local maxima for chiral d -wave SC even in the presence of the spin-dependent barrier. This shows that the charge conductance of the junction is available for the distinction between chiral p -wave SC and chiral d -wave one.

IV. CONCLUSION

In this paper, we have studied the tunneling conductance between two-dimensional p -wave altermagnet(AM) / superconductor (SC) junctions. We choose various types of pairing symmetries of superconductors such as s -wave, $d_{x^2-y^2}$ -wave, d_{xy} -wave, p_x -wave, p_y -wave, chiral p -wave, and chiral d -wave pairings. The zero bias conductance peak due to the zero energy surface Andreev bound states (ZESABS) in d_{xy} -wave and p_x -wave superconductor

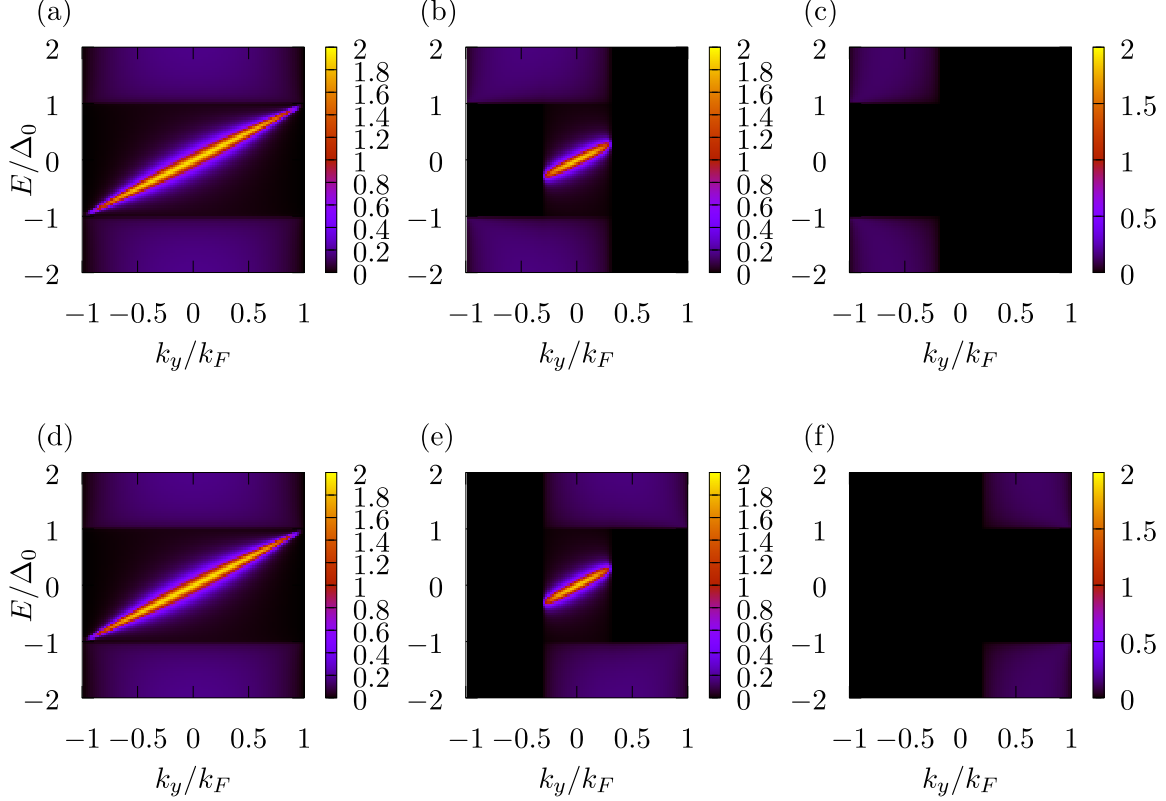


FIG. 15. Momentum resolved conductance $\sigma_{\uparrow}^S(E, k_y)$ ((a),(b),(c)) and $\sigma_{\downarrow}^S(E, k_y)$ ((d),(e),(f)) for p_y -wave altermagnet/Insulator/chiral p -wave superconductor with $d \parallel \hat{x}$ junction where $Z = 2$. The strength of p -wave altermagnet is set to $\tilde{\alpha}_y = 0$ ((a),(d)), 0.7 ((b),(e)), and 1.2 ((c),(f)). The number of chiral-edge mode is $N = 1$ and the values of M and k_1 in Eq. (48) becomes $M = 1$ and $k_1/k_F = 0$.

junctions are insensitive against the change of α_y which is an indicator of the magnitude of the momentum-dependent band splitting. Changing the orientation of p -wave AM has the same effect as changing the strength of the AM. For chiral- p or chiral- d wave SCs, zero bias conductance shows a non-monotonic change as a function of the strength of altermagnet since the surface Andreev bound states have a momentum dependence. The tunneling spectroscopy based on a p -wave altermagnet can be a useful way to detect the SABS with momentum dependence. It is noted that our obtained conductance formula is available for persistent spin-helix / SC junctions since p -wave altermagnetism is essentially equivalent to the persistent spin-helix system.

It is also noted that theoretical works about the superconducting diode effect in altermagnetic junctions⁷⁴ and orientationally dependence on Josephson current in spin-triplet

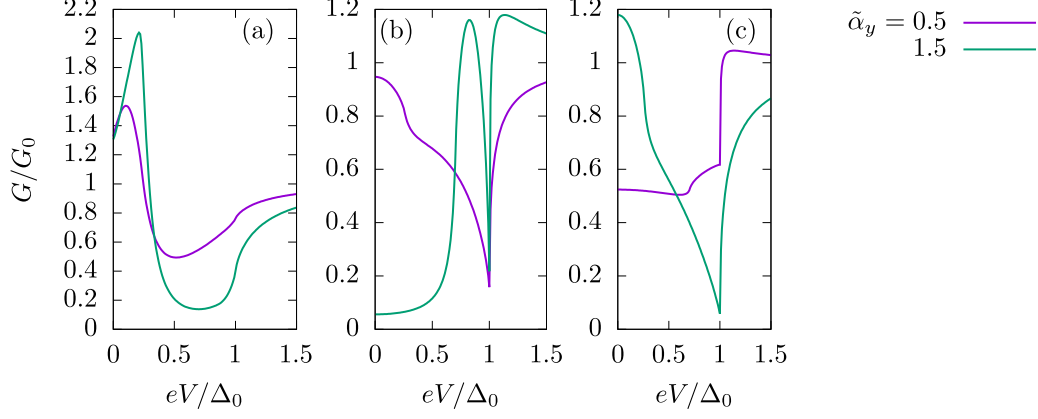


FIG. 16. Normalized conductance G/G_0 of p_y -wave altermagnet/Ferromagnetic Insulator/superconductor junctions. The barrier is set to $Z_\uparrow = 1, Z_\downarrow = 3$. (a) d_{xy} -wave SC. (b)chiral p -wave SC with $\mathbf{d} \parallel \hat{\mathbf{z}}$. (c)chiral d -wave SC.

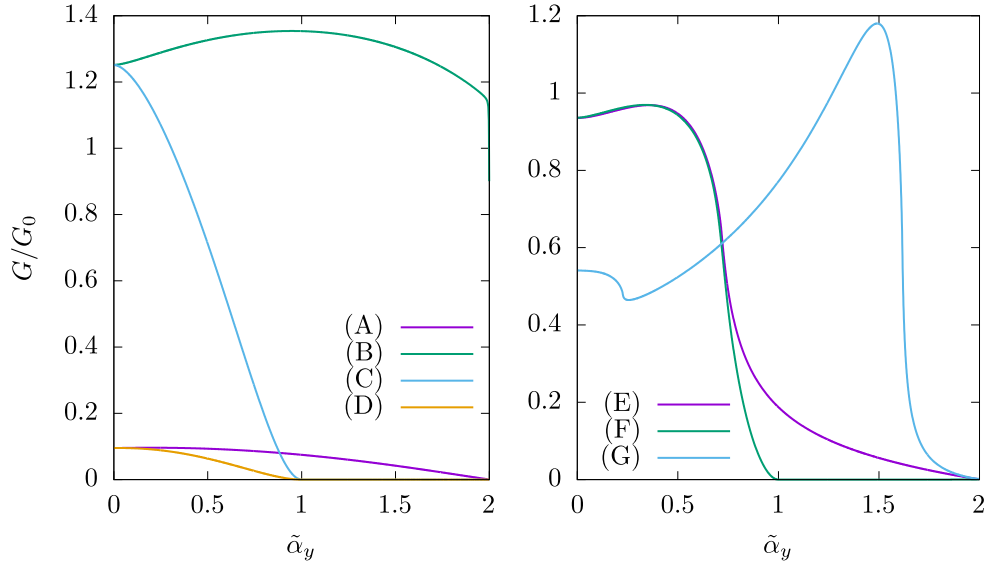


FIG. 17. The α_y dependency of zero bias conductance at $Z_\uparrow = 1, Z_\downarrow = 3$. (A) s -wave, p_y -wave with $\mathbf{d} \parallel \hat{\mathbf{z}}$, $d_{x^2-y^2}$ -wave, (B) p_x -wave with $\mathbf{d} \parallel \hat{\mathbf{z}}$, d_{xy} -wave, (C) p_x -wave with $\mathbf{d} \parallel \hat{\mathbf{x}}$, (D) p_y -wave with $\mathbf{d} \parallel \hat{\mathbf{x}}$, (E)chiral p -wave with $\mathbf{d} \parallel \hat{\mathbf{z}}$, (F)chiral p -wave with $\mathbf{d} \parallel \hat{\mathbf{x}}$, and (G)chiral d -wave.

superconductor junction has been started⁷⁵. As a future work, it is interesting to study the Josephson effect involving altermagnet and unconventional superconductors because the presence of ZESABS seriously influences on the current phase relation and temperature dependence of the Josephson current^{47,76,77}. Also, it is intriguing to clarify the impact of ferromagnetic insulator at the interface in these junctions.^{78,79}

V. ACKNOWLEDGEMENTS

We thank S. Ikegaya for the valuable information and constructive discussion. We also thank J. Linder, S. Kashiwaya, D. Hirai, and S. Onari, for their discussions. Y. T. acknowledges support from JSPS with Grants-in-Aid for Scientific Research (KAKENHI Grants No. 20H00131 and No. 23K17668).

Appendix A: Wave functions in the superconductor

In this section, we introduce the wave functions in spin-singlet SC or spin-triplet SC with a \mathbf{d} -vector parallel to the z -axis based on the standard theory of tunneling spectroscopy of unconventional superconductors⁴⁷. The wave function in SC can be written as

$$\Psi_{\uparrow}(x, k_y) = t_{\uparrow} \begin{pmatrix} 1 \\ 0 \\ 0 \\ \Gamma_+ \end{pmatrix} e^{ik_e^s x} + t_{\uparrow}^A \begin{pmatrix} \Gamma_- \\ 0 \\ 0 \\ 1 \end{pmatrix} e^{-ik_h^s x} \quad (\text{A1})$$

$$\Psi_{\downarrow}(x, k_y) = t_{\downarrow} \begin{pmatrix} 0 \\ 1 \\ \mp\Gamma_+ \\ 0 \end{pmatrix} e^{ik_e^s x} + t_{\downarrow}^A \begin{pmatrix} 0 \\ \mp\Gamma_- \\ 1 \\ 0 \end{pmatrix} e^{-ik_h^s x} \quad (\text{A2})$$

where $\rho = \uparrow, \downarrow$ denotes the spin index of an injected electron. In Eq. (A2), the sign \mp becomes $-$ for spin-singlet SC and $+$ for spin-triplet SC, respectively. In the above, we have used the following relations

$$k_e^s = \sqrt{\frac{2m}{\hbar^2} (\mu + \Omega_+) - k_y^2}, \quad (\text{A3})$$

$$k_h^s = \sqrt{\frac{2m}{\hbar^2} (\mu - \Omega_-) - k_y^2}. \quad (\text{A4})$$

Appendix B: Independence of the transparency by α_x

The k_y -resolved transparencies of p -AM/SC and p -AM/normal metal junctions $\sigma_{\uparrow(\downarrow)}^N(E, k_y)$ and $\sigma_{\uparrow(\downarrow)}^N(E, k_y)$ are independent of α_x since

$$\check{v}_x \Psi_{\uparrow}(x = 0_-, k_y) = \frac{\hbar k_F}{m} \begin{pmatrix} q_{e\uparrow}^+ + r_{\uparrow} q_{e\uparrow}^- \\ 0 \\ 0 \\ r_{\uparrow}^A q_{h\downarrow}^- \end{pmatrix} \quad (\text{B1})$$

$$\check{v}_x \Psi_{\downarrow}(x = 0_-, k_y) = \frac{\hbar k_F}{m} \begin{pmatrix} 0 \\ q_{e\downarrow}^+ + r_{\downarrow} q_{e\downarrow}^- \\ r_{\downarrow}^A q_{h\uparrow}^- \\ 0 \end{pmatrix} \quad (\text{B2})$$

$$\check{v}_x \Psi_{\uparrow}(x = 0_+, k_y) = \frac{\hbar k_F}{m} \begin{pmatrix} t_{\uparrow} k_e^s - t_{\uparrow}^A k_h^s \Gamma_- \\ 0 \\ 0 \\ -t_{\uparrow} k_e^s \Gamma_+ + t_{\uparrow}^A k_h^s \end{pmatrix} \quad (\text{B3})$$

$$\check{v}_x \Psi_{\downarrow}(x = 0_+, k_y) = \frac{\hbar k_F}{m} \begin{pmatrix} 0 \\ t_{\downarrow} k_e^s \pm t_{\downarrow}^A k_h^s \Gamma_- \\ \pm t_{\downarrow} k_e^s \Gamma_+ + t_{\downarrow}^A k_h^s \\ 0 \end{pmatrix} \quad (\text{B4})$$

based on Eq. (13) where $q_{e\uparrow(\downarrow)}^{\pm}$, $q_{h\uparrow(\downarrow)}^{\pm}$, k_e^s , and k_h^s are independent of α_x , with which Eqs. (11) and (12) yields $r_{\uparrow(\downarrow)}$ and $r_{\uparrow(\downarrow)}^A$ independent of α_x .

Appendix C: Comparison with d -wave altermagnet

In this section, we consider a d -wave AM / Insulator (I) / SC junction for comparison with the p -wave AM case. The corresponding BdG Hamiltonian in the system can be written by 4×4 matrix as follows:

$$\check{\mathcal{H}}_{\text{BdG}} = \begin{bmatrix} \hat{h}(\mathbf{k}, x) & \hat{\Delta}(\hat{\mathbf{k}}) \Theta(x) \\ -\hat{\Delta}^*(-\hat{\mathbf{k}}) \Theta(x) & -\hat{h}^*(-\mathbf{k}, x) \end{bmatrix} \quad (\text{C1})$$

where the single-particle Hamiltonian $\hat{h}(\mathbf{k}, x)$ can be written as¹⁷

$$\hat{h}(\mathbf{k}, x) = \text{diag}(\xi_+(\mathbf{k}, x), \xi_-(\mathbf{k}, x)) + \hat{U}_0 \delta(x) \quad (\text{C2})$$

$$\xi_{\pm} = \frac{\hbar^2}{2m} \mathbf{k}^2 \pm \left[\alpha_1 k_x k_y + \frac{\alpha_2}{2} (k_x^2 - k_y^2) \right] \Theta(x) - \mu. \quad (\text{C3})$$

Here, 2×2 matrix \hat{U}_0 given by

$$\hat{U}_0 = U \hat{I}, \hat{I} = \text{diag}(1, 1) \quad (\text{C4})$$

denotes the insulating barrier at $x = 0$. Here, the shapes of the polarized Fermi surfaces for spin- \uparrow and spin- \downarrow electron species are changed differently by parameters α_1 and α_2 . We define a dimensionless parameter $Z = mU/(\hbar^2 k_F)$ with k_F being the Fermi wave vector on the superconducting side. In the d -wave AM region $x < 0$, the x -components of the possible wave vectors for fixed E and k_y are given by

$$k_{e\uparrow}^{\pm} = k_F \left[\pm \frac{1}{1 + \tilde{\alpha}_2} \sqrt{\left(1 + \frac{E}{\mu}\right) (1 + \tilde{\alpha}_2) + \tilde{k}_y^2 (\tilde{\alpha}_1^2 + \tilde{\alpha}_2^2 - 1)} - \frac{\tilde{\alpha}_1}{1 + \tilde{\alpha}_2} \tilde{k}_y \right], \quad (\text{C5})$$

$$k_{e\downarrow}^{\pm} = k_F \left[\pm \frac{1}{1 - \tilde{\alpha}_2} \sqrt{\left(1 + \frac{E}{\mu}\right) (1 - \tilde{\alpha}_2) + \tilde{k}_y^2 (\tilde{\alpha}_1^2 + \tilde{\alpha}_2^2 - 1)} + \frac{\tilde{\alpha}_1}{1 - \tilde{\alpha}_2} \tilde{k}_y \right], \quad (\text{C6})$$

$$k_{h\uparrow}^{\mp} = k_F \left[\mp \frac{1}{1 + \tilde{\alpha}_2} \sqrt{\left(1 - \frac{E}{\mu}\right) (1 + \tilde{\alpha}_2) + \tilde{k}_y^2 (\tilde{\alpha}_1^2 + \tilde{\alpha}_2^2 - 1)} - \frac{\tilde{\alpha}_1}{1 + \tilde{\alpha}_2} \tilde{k}_y \right], \quad (\text{C7})$$

$$k_{h\downarrow}^{\mp} = k_F \left[\mp \frac{1}{1 - \tilde{\alpha}_2} \sqrt{\left(1 - \frac{E}{\mu}\right) (1 - \tilde{\alpha}_2) + \tilde{k}_y^2 (\tilde{\alpha}_1^2 + \tilde{\alpha}_2^2 - 1)} + \frac{\tilde{\alpha}_1}{1 - \tilde{\alpha}_2} \tilde{k}_y \right], \quad (\text{C8})$$

with dimensionless parameters $\tilde{\alpha}_1 = m\alpha_1/\hbar^2$, $\tilde{\alpha}_2 = m\alpha_2/\hbar^2$, and $\tilde{k}_y = k_y/k_F$. Here, like Eqs. (15)–(18), the subscripts e and h correspond to an electron and a hole respectively, \uparrow, \downarrow denote the spin, and the superscripts \pm correspond to the sign of the eigenvalues of the velocity operator

$$\check{v}_x = \frac{1}{\hbar} \frac{\partial \check{\mathcal{H}}_{\text{BdG}}}{\partial k_x} = \tilde{\tau}_z \left[\frac{\hbar}{m} + \tilde{\sigma}_z \frac{\alpha_2}{\hbar} \Theta(-x) \right] \frac{1}{i} \frac{\partial}{\partial x} + \tilde{\tau}_z \tilde{\sigma}_z \frac{\alpha_1}{\hbar} k_y \Theta(-x). \quad (\text{C9})$$

From the Hamiltonian Eq. C1, we obtain wavefunctions $\Psi(x, y) = \Psi(x, k_y) e^{ik_y y}$ which follows the boundary condition

$$\Psi(x, k_y) \Big|_{x=0_+} = \Psi(x, k_y) \Big|_{x=0_-}, \quad (\text{C10})$$

$$\check{v}_x \Psi(x, k_y) \Big|_{x=0_+} - \check{v}_x \Psi(x, k_y) \Big|_{x=0_-} = \frac{2U}{i\hbar} \check{\tau}_3 \Psi(0, k_y). \quad (\text{C11})$$

The scattering coefficients as well as the conductance can thus be solved following the same way in the main text.

It is noted that the strength of AM must satisfy $|\tilde{\alpha}_1^2 + \tilde{\alpha}_2^2| < 1$ to keep the Fermi surface $E = 0$ in a restricted domain in the momentum space. In the same way as Eqs. (43)–(47), we get the conditions for injected electrons with a particular value of k_y to contribute to the conduction process with $|E| \ll \mu$ as follows. In the case of $|E| > |\Delta(\theta_{\pm})|$, the condition for a spin- \uparrow (\downarrow) electron can be approximately rewritten as

$$|k_y| < k_{\uparrow(\downarrow)}^c, \quad (\text{C12})$$

with

$$\frac{k_{\uparrow}^c}{k_F} = \min \left(1, \sqrt{\frac{1 + \tilde{\alpha}_2}{1 - \tilde{\alpha}_1^2 - \tilde{\alpha}_2^2}} \right), \quad \frac{k_{\downarrow}^c}{k_F} = \min \left(1, \sqrt{\frac{1 - \tilde{\alpha}_2}{1 - \tilde{\alpha}_1^2 - \tilde{\alpha}_2^2}} \right). \quad (\text{C13})$$

For $|E| < |\Delta(\theta_{\pm})|$, in the cases of spin-singlet pairing or spin-triplet pairing with $\mathbf{d} \parallel \hat{z}$, the wave vector of the reflected spin- \downarrow (\uparrow) hole is nearly equivalent to that of a spin- \downarrow (\uparrow) electron and the condition in Eq. (C12) changes into

$$|k_y| < k^c, \quad (\text{C14})$$

with

$$\frac{k^c}{k_F} = \min \left(1, \sqrt{\frac{1 + \tilde{\alpha}_2}{1 - \tilde{\alpha}_1^2 - \tilde{\alpha}_2^2}}, \sqrt{\frac{1 - \tilde{\alpha}_2}{1 - \tilde{\alpha}_1^2 - \tilde{\alpha}_2^2}} \right), \quad (\text{C15})$$

for both an injected spin- \uparrow electron and a spin- \downarrow one. On the other hand, in the case of spin-triplet pairing with $\mathbf{d} \parallel \hat{x}$, the wave vector of the reflected spin- \uparrow (\downarrow) hole is nearly equivalent to that of a spin- \uparrow (\downarrow) electron and the condition in Eq. (C12) does not change. It is noted that, for the d_{xy} -wave AM case with $\tilde{\alpha}_2 = 0$, both the conditions in Eqs. (C12) and (C14) can be simply written as $|k_y| < k_F$.

To compare the behaviors of p -wave altermagnet and d -wave one, we calculate the normalized conductance G/G_0 of d -wave AM/I/SC junctions at $eV = 0$ as functions of $\tilde{\alpha}_1$ or $\tilde{\alpha}_2$ as shown in Figs. 18 and 19. We set $\tilde{\alpha}_2 = 0$ for d_{xy} -wave AM and $\tilde{\alpha}_1 = 0$ for $d_{x^2-y^2}$ -wave AM in Figs. 18 and 19, respectively. As compared to the p_y -wave AM where the normalized conductance G/G_0 develops a drastic change with the strength of AM, G/G_0 shows only a slight variation with the increase of the strength of AM $|\tilde{\alpha}_1|$ for the d_{xy} -wave AM. Similarly,

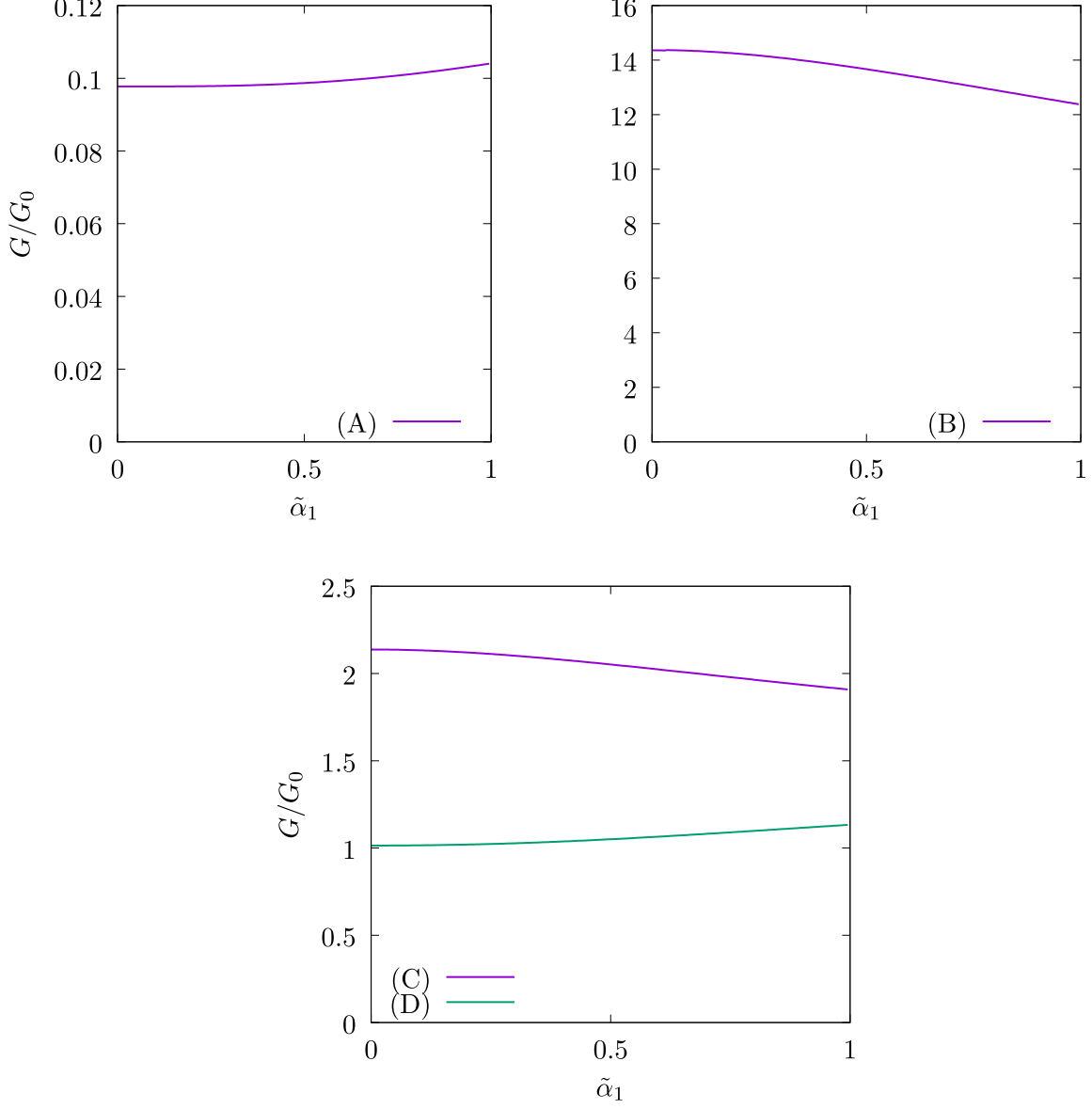


FIG. 18. The $\tilde{\alpha}_1$ dependence of zero bias conductance of d_{xy} -wave AM/I/SC junctions at $Z = 2$. The pairing symmetry of SCs are (A) s -wave, p_y -wave with $\mathbf{d} \parallel \hat{z}$, p_y -wave with $\mathbf{d} \parallel \hat{x}$, $d_{x^2-y^2}$ -wave, (B) p_x -wave with $\mathbf{d} \parallel \hat{z}$, p_x -wave with $\mathbf{d} \parallel \hat{x}$, d_{xy} -wave, (C)chiral p -wave with $\mathbf{d} \parallel \hat{z}$, chiral p -wave with $\mathbf{d} \parallel \hat{x}$, and (D)chiral d -wave.

the variation of G/G_0 is small for spin-triplet SC with $\mathbf{d} \parallel \hat{x}$ in the $d_{x^2-y^2}$ -wave AM case with the increase of $|\tilde{\alpha}_2|$. In these cases, the condition of k_y becomes the same for the normal state and the superconducting state. In addition, the x -components of the group velocities of electrons and holes in AM are even functions of k_y as well as those in SC, which we can derive from Eqs. (C5)–(C9). As a consequence, the discrepancy among the group velocities

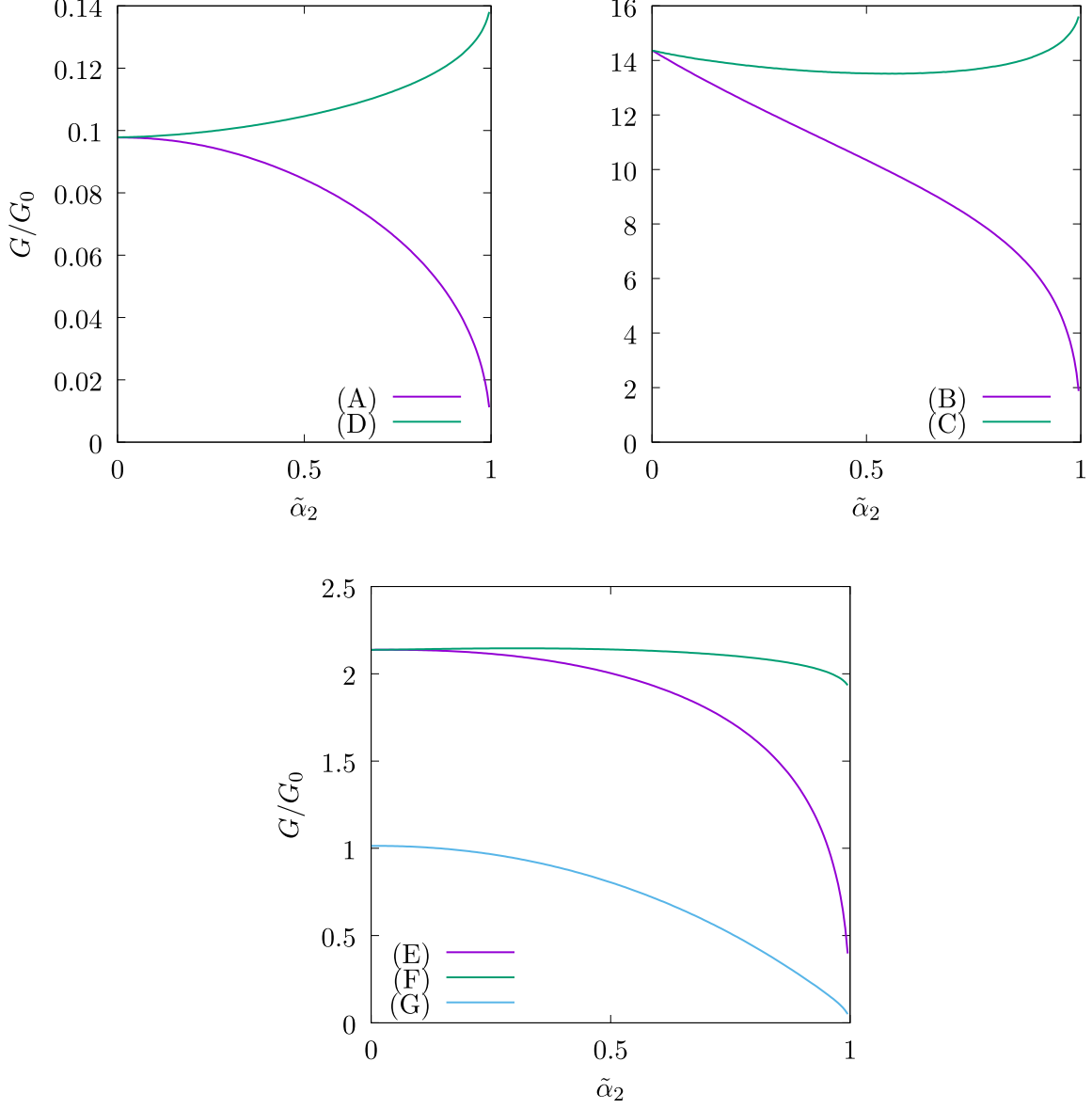


FIG. 19. The $\tilde{\alpha}_2$ dependence of zero bias conductance of $d_{x^2-y^2}$ -wave AM/I/SC junctions at $Z = 2$. The pairing symmetry of SCs are (A) s -wave, p_y -wave with $\mathbf{d} \parallel \hat{\mathbf{z}}$, $d_{x^2-y^2}$ -wave, (B) p_x -wave with $\mathbf{d} \parallel \hat{\mathbf{z}}$, d_{xy} -wave, (C) p_x -wave with $\mathbf{d} \parallel \hat{\mathbf{x}}$, (D) p_y -wave with $\mathbf{d} \parallel \hat{\mathbf{x}}$, (E)chiral p -wave with $\mathbf{d} \parallel \hat{\mathbf{z}}$, (F)chiral p -wave with $\mathbf{d} \parallel \hat{\mathbf{x}}$, and (G)chiral d -wave.

for electrons and holes in AM and SC becomes smaller than that in the p_y -wave AM case and the root of the boundary conditions in Eqs. (11) and (12) does not change significantly with $\tilde{\alpha}_1$ or $\tilde{\alpha}_2$. By contrast, for $d_{x^2-y^2}$ -wave AM/I/SC junctions with spin-singlet SC or spin-triplet one with $\mathbf{d} \parallel \hat{\mathbf{z}}$, G/G_0 is strongly suppressed with the increase of $|\tilde{\alpha}_2|$. In this case, the range of k_y contributing to the conduction process is restricted similarly for the

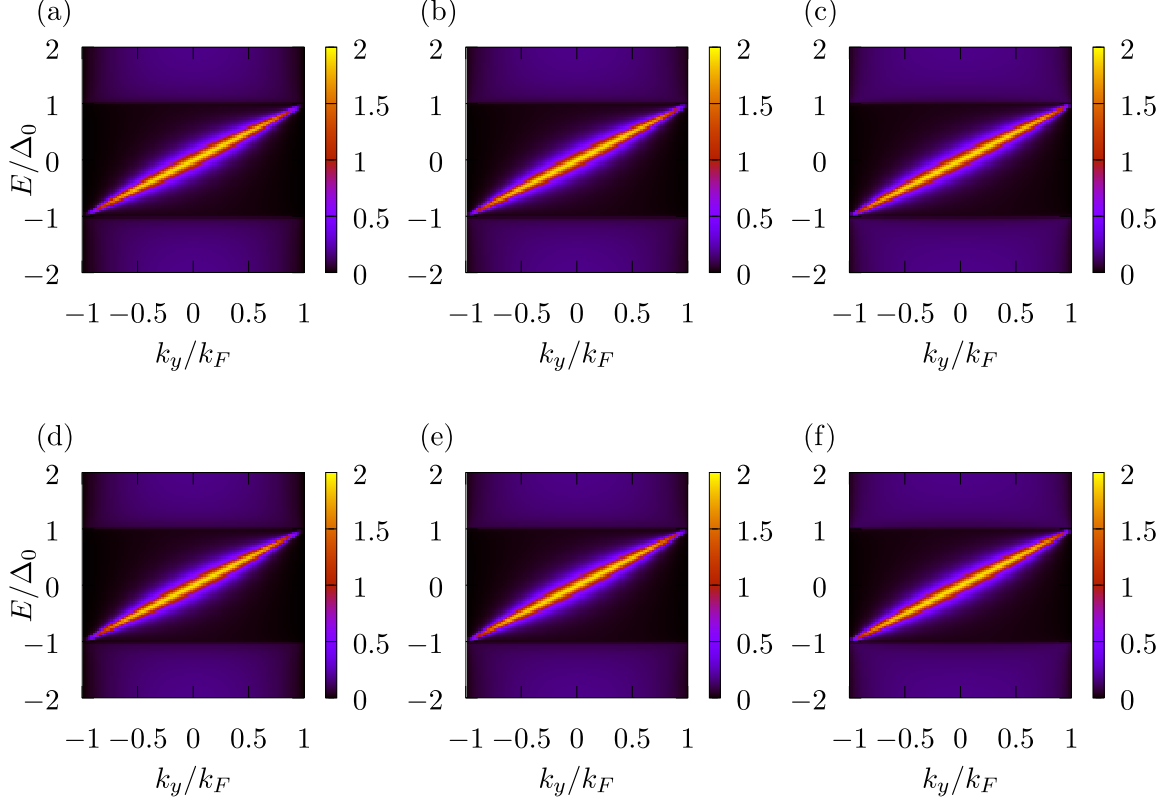


FIG. 20. Momentum resolved conductance $\sigma_{\uparrow}^S(E, k_y)$ ((a),(b),(c)) and $\sigma_{\downarrow}^S(E, k_y)$ ((d),(e),(f)) for d_{xy} -wave altermagnet/Insulator/chiral p -wave superconductor with $\mathbf{d} \parallel \hat{\mathbf{z}}$ junction where $Z = 2$. The strength of altermagnet is set to $\tilde{\alpha}_1 = 0$ ((a),(d)), 0.5 ((b),(e)), and 0.9 ((c),(f)).

spin- \uparrow electron injection and that of spin- \downarrow with $|E| < \Delta(\theta_{\pm})$ for the superconducting state. By contrast, for the normal state, the range of k_y is merely $|k_y| < k_F$ with $\tilde{\alpha}_2 > 0$ ($\tilde{\alpha}_2 < 0$) for the spin- \uparrow (\downarrow) electron injection.

It is noted that G/G_0 for chiral SC as a function of $\tilde{\alpha}_1, \tilde{\alpha}_2$ does not have conspicuous local maxima or local minima like those in the p -wave AM cases shown in Figs. 11, 12 and 17. To clarify this difference, we calculate the k_y - and spin-resolved conductance $\sigma_{\uparrow}^S(E, k_y)$ and $\sigma_{\downarrow}^S(E, k_y)$ of d -AM/I/chiral SC junctions as shown in Figs. 20–23. Figure 20 is an example of the d_{xy} -AM cases and shows the change of $\sigma_{\uparrow(\downarrow)}^S(E, k_y)$ by $\tilde{\alpha}_1$ is small for all k_y . For the $d_{x^2-y^2}$ -AM cases, as shown in Figs. 21–23, the range of k_y contributing to the conduction process is changed by $\tilde{\alpha}_2$ following Eqs. (C12) and (C14). This range cannot be narrower than $|k_y|/k_F < 1/\sqrt{2}$ with $|\tilde{\alpha}_2| < 1$ and the boundaries of the momentum parallel to the interface $k^c, k_{\uparrow(\downarrow)}^c$ do not cross the chiral edge modes at $E = 0$ for chiral p - and d -wave SCs. As a consequence, any prominent local maxima of G/G_0 as a function of $\tilde{\alpha}_2$ cannot be seen

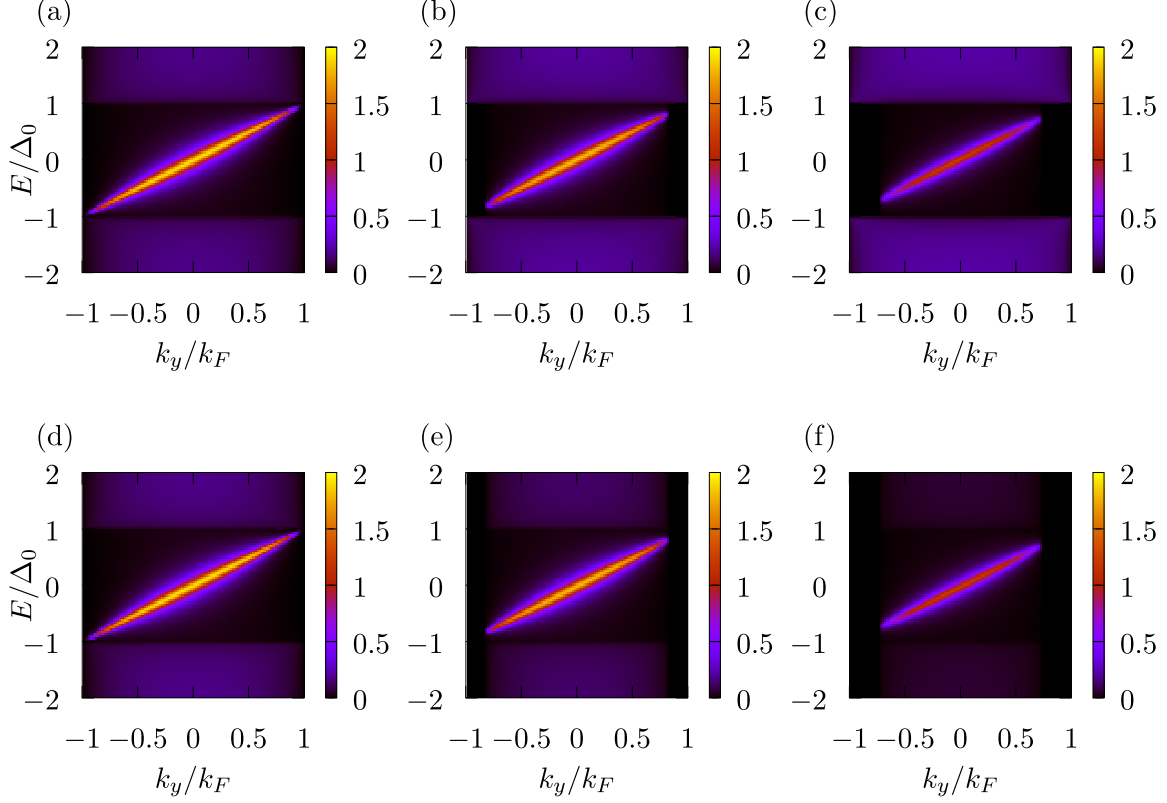


FIG. 21. Momentum resolved conductance $\sigma_{\uparrow}^S(E, k_y)$ ((a),(b),(c)) and $\sigma_{\downarrow}^S(E, k_y)$ ((d),(e),(f)) for $d_{x^2-y^2}$ -wave altermagnet/Insulator/chiral p -wave superconductor with $\mathbf{d} \parallel \hat{z}$ junction where $Z = 2$. The strength of altermagnet is set to $\tilde{\alpha}_2 = 0$ ((a),(d)), 0.5 ((b),(e)), and 0.9 ((c),(f)).

in the $d_{x^2-y^2}$ -AM case. The discussion above indicates that the asymmetric restriction of k_y and the boundary of k_y reaching $k_y = 0$ as shown in Figs. 13–15 are important features of p -wave AM compared to d -wave AM.

-
- ¹ L. Šmejkal, R. González-Hernández, T. Jungwirth, and J. Sinova, *Sci. Adv.* **6**, eaaz8809 (2020).
² L. Šmejkal, J. Sinova, and T. Jungwirth, *Phys. Rev. X* **12**, 031042 (2022).
³ S. Hayami, Y. Yanagi, and H. Kusunose, *J. Phys. Soc. Jpn.* **88**, 123702 (2019).
⁴ S. Hayami, Y. Yanagi, and H. Kusunose, *Phys. Rev. B* **102**, 144441 (2020).
⁵ L. Šmejkal, J. Sinova, and T. Jungwirth, *Phys. Rev. X* **12**, 040501 (2022).
⁶ I. I. Mazin, K. Koepernik, M. D. Johannes, R. González-Hernández, and L. Šmejkal, *Proc. Natl. Acad. Sci. U.S.A.* **118**, e2108924118 (2021).

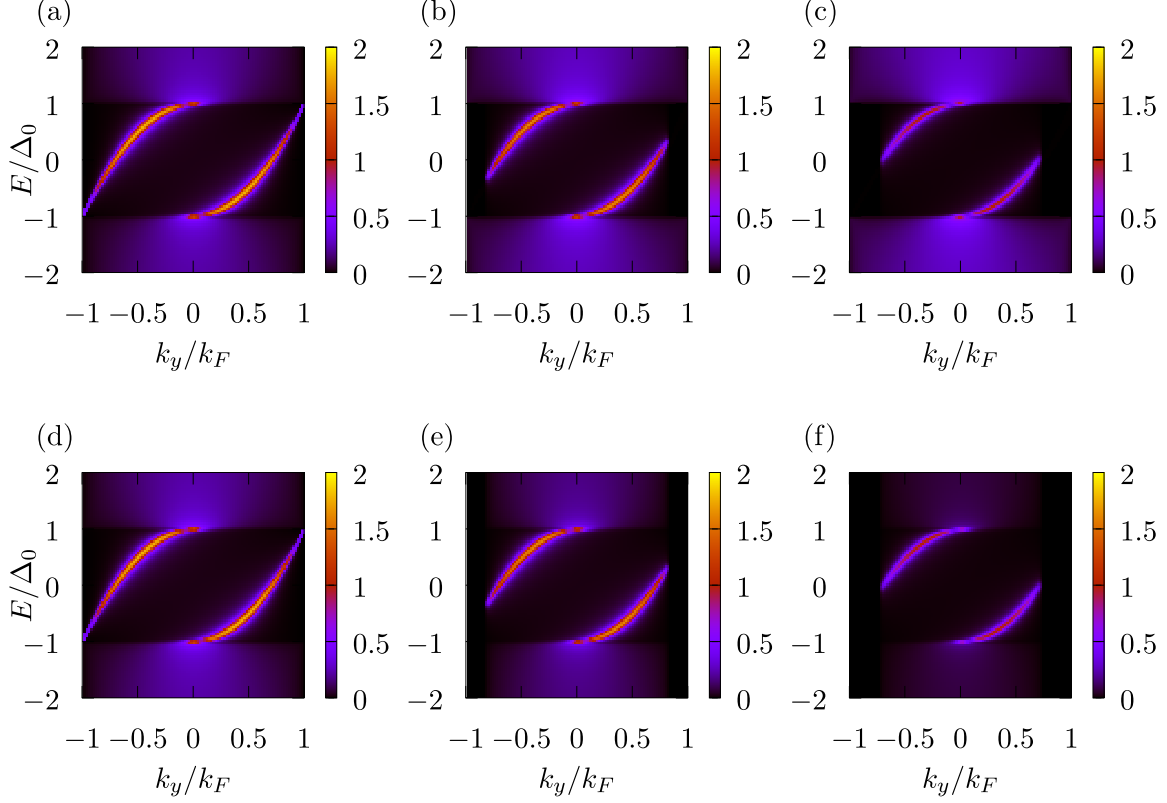


FIG. 22. Momentum resolved conductance $\sigma_{\uparrow}^S(E, k_y)$ ((a),(b),(c)) and $\sigma_{\downarrow}^S(E, k_y)$ ((d),(e),(f)) for $d_{x^2-y^2}$ -wave altermagnet/Insulator/chiral d -wave superconductor junction where $Z = 2$. The strength of altermagnet is set to $\tilde{\alpha}_2 = 0$ ((a),(d)), 0.5 ((b),(e)), and 0.9 ((c),(f)).

- ⁷ I. Mazin (The PRX Editors), Phys. Rev. X **12**, 040002 (2022).
- ⁸ L. Šmejkal, A. B. Hellenes, R. González-Hernández, J. Sinova, and T. Jungwirth, Phys. Rev. X **12**, 011028 (2022).
- ⁹ K.-H. Ahn, A. Hariki, K.-W. Lee, and J. Kuneš, Phys. Rev. B **99**, 184432 (2019).
- ¹⁰ O. Fedchenko, J. Minár, A. Akashdeep, S. W. D'Souza, D. Vasilyev, O. Tkach, L. Odenbreit, Q. Nguyen, D. Kutnyakhov, N. Wind, L. Wenthaus, M. Scholz, K. Rossnagel, M. Hoesch, M. Aeschlimann, B. Stadtmüller, M. Kläui, G. Schönhense, T. Jungwirth, A. B. Hellenes, G. Jakob, L. Šmejkal, J. Sinova, and H.-J. Elmers, Sci. Adv. **10**, eadj4883 (2024).
- ¹¹ S. Lee, S. Lee, S. Jung, J. Jung, D. Kim, Y. Lee, B. Seok, J. Kim, B. G. Park, L. Šmejkal, C.-J. Kang, and C. Kim, Phys. Rev. Lett. **132**, 036702 (2024).
- ¹² T. Osumi, S. Souma, T. Aoyama, K. Yamauchi, A. Honma, K. Nakayama, T. Takahashi, K. Ohgushi, and T. Sato, (2024), arXiv:2308.10117.

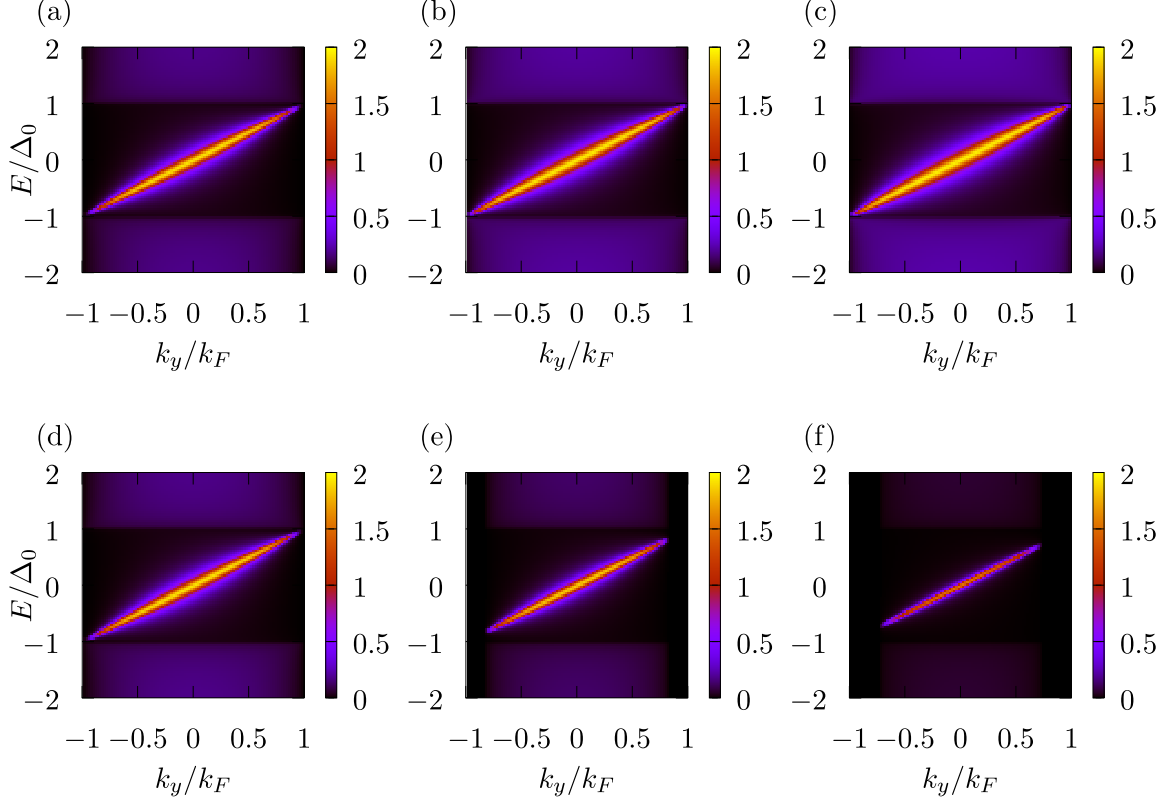


FIG. 23. Momentum resolved conductance $\sigma_{\uparrow}^S(E, k_y)$ ((a),(b),(c)) and $\sigma_{\downarrow}^S(E, k_y)$ ((d),(e),(f)) for $d_{x^2-y^2}$ -wave altermagnet/Insulator/chiral p -wave superconductor with $\mathbf{d} \parallel \hat{x}$ junction where $Z = 2$. The strength of altermagnet is set to $\tilde{\alpha}_2 = 0$ ((a),(d)), 0.5((b),(e)), and 0.9((c),(f)).

¹³ J. Krempaský, L. Šmejkal, S. W. D'Souza, M. Hajlaoui, G. Springholz, K. Uhlířová, F. Alarab, P. C. Constantinou, V. Strocov, D. Usanov, W. R. Pudelko, R. González-Hernández, A. Birk Hellenes, Z. Jansa, H. Reichlová, Z. Šobáň, R. D. Gonzalez Betancourt, P. Wadley, J. Sinova, D. Kriegner, J. Minár, J. H. Dil, and T. Jungwirth, *Nature* **626**, 517 (2024).

¹⁴ H. Reichlová, R. L. Seeger, R. González-Hernández, I. Kounta, R. Schlitz, D. Kriegner, P. Ritzinger, M. Lammel, M. Leiviskä, V. Petříček, P. Doležal, E. Schmoranzarová, A. Bad'ura, A. Thomas, V. Baltz, L. Michez, J. Sinova, S. T. B. Goennenwein, T. Jungwirth, and L. Šmejkal, (2021), arXiv:2012.15651.

¹⁵ S. López-Moreno, A. H. Romero, J. Mejía-López, and A. Muñoz, *Phys. Chem. Chem. Phys.* **18**, 33250 (2016).

¹⁶ C. W. J. Beenakker and T. Vakhtel, *Phys. Rev. B* **108**, 075425 (2023).

¹⁷ C. Sun, A. Brataas, and J. Linder, *Phys. Rev. B* **108**, 054511 (2023).

- ¹⁸ M. Papaj, Phys. Rev. B **108**, L060508 (2023).
- ¹⁹ J. A. Ouassou, A. Brataas, and J. Linder, Phys. Rev. Lett. **131**, 076003 (2023).
- ²⁰ T. N. Song-Bo Zhang, Lun-Hui Hu, (2023), arXiv:2302.13185.
- ²¹ Y. Nagae, A. P. Schnyder, and S. Ikegaya, (2024), arXiv:2403.07117.
- ²² B. Lu, K. Maeda, H. Ito, K. Yada, and Y. Tanaka, arXiv preprint arXiv:2405.10656 (2024).
- ²³ A. I. Buzdin, Reviews of modern physics **77**, 935 (2005).
- ²⁴ F. Bergeret, A. F. Volkov, and K. B. Efetov, Reviews of modern physics **77**, 1321 (2005).
- ²⁵ J. Linder and J. W. Robinson, Nature Physics **11**, 307 (2015).
- ²⁶ M. Eschrig, Reports on Progress in Physics **78**, 104501 (2015).
- ²⁷ H. G. Giil and J. Linder, (2023), arXiv:2308.10939.
- ²⁸ S. A. A. Ghorashi, T. L. Hughes, and J. Cano, (2023), arXiv:2306.09413.
- ²⁹ D. Zhu, Z.-Y. Zhuang, Z. Wu, and Z. Yan, Phys. Rev. B **108**, 184505 (2023).
- ³⁰ I. Bobkova, P. Hirschfeld, and Y. S. Barash, arXiv preprint cond-mat/0408032 (2004).
- ³¹ B. M. Andersen, I. Bobkova, P. Hirschfeld, and Y. S. Barash, Physical Review B **72**, 184510 (2005).
- ³² M. F. Jakobsen, K. B. Naess, P. Dutta, A. Brataas, and A. Qaiumzadeh, Physical Review B **102**, 140504 (2020).
- ³³ M. F. Jakobsen, A. Brataas, and A. Qaiumzadeh, Physical Review Letters **127**, 017701 (2021).
- ³⁴ G. E. Blonder, M. Tinkham, and T. Klapwijk, Phys. Rev. B **25**, 4515 (1982).
- ³⁵ Y. Tanaka and S. Kashiwaya, Phys. Rev. Lett. **74**, 3451 (1995).
- ³⁶ S. Kashiwaya, Y. Tanaka, M. Koyanagi, and K. Kajimura, Phys. Rev. B **53**, 2667 (1996).
- ³⁷ M. Sato, Y. Tanaka, K. Yada, and T. Yokoyama, Phys. Rev. B **83**, 224511 (2011).
- ³⁸ A. P. Schnyder and S. Ryu, Phys. Rev. B **84**, 060504 (2011).
- ³⁹ P. M. R. Brydon, A. P. Schnyder, and C. Timm, Phys. Rev. B **84**, 020501 (2011).
- ⁴⁰ S. Matsuura, P.-Y. Chang, A. P. Schnyder, and S. Ryu, New Journal of Physics **15**, 065001 (2013).
- ⁴¹ S. Kobayashi, K. Shiozaki, Y. Tanaka, and M. Sato, Phys. Rev. B **90**, 024516 (2014).
- ⁴² S. Kobayashi, Y. Yanase, and M. Sato, Phys. Rev. B **94**, 134512 (2016).
- ⁴³ S. Kobayashi, S. Sumita, Y. Yanase, and M. Sato, Phys. Rev. B **97**, 180504(R) (2018).
- ⁴⁴ Y. Tanaka, M. Sato, and N. Nagaosa, Journal of the Physical Society of Japan **81**, 011013 (2011).

- ⁴⁵ Y. Tanaka, S. Tamura, and J. Cayao, Progress of Theoretical and Experimental Physics ,
ptae065 (2024).
- ⁴⁶ M. Yamashiro, Y. Tanaka, Y. Tanuma, and S. Kashiwaya, J. Phys. Soc. Jpn. **67**, 3224 (1998).
- ⁴⁷ S. Kashiwaya and Y. Tanaka, Rep. Prog. Phys. **63**, 1641 (2000).
- ⁴⁸ C.-R. Hu, Phys. Rev. Lett. **72**, 1526 (1994).
- ⁴⁹ L. Alff, H. Takashima, S. Kashiwaya, N. Terada, H. Ihara, Y. Tanaka, M. Koyanagi, and
K. Kajimura, Phys. Rev. B **55**, R14757 (1997).
- ⁵⁰ J. Y. T. Wei, N.-C. Yeh, D. F. Garrigus, and M. Strasik, Phys. Rev. Lett. **81**, 2542 (1998).
- ⁵¹ I. Iguchi, W. Wang, M. Yamazaki, Y. Tanaka, and S. Kashiwaya, Phys. Rev. B **62**, R6131
(2000).
- ⁵² M. Covington, M. Aprili, E. Paraoanu, L. H. Greene, F. Xu, J. Zhu, and C. A. Mirkin, Phys.
Rev. Lett. **79**, 277 (1997).
- ⁵³ J. Y. T. Wei, N.-C. Yeh, D. F. Garrigus, and M. Strasik, Phys. Rev. Lett. **81**, 2542 (1998).
- ⁵⁴ A. Biswas, P. Fournier, M. M. Qazilbash, V. N. Smolyaninova, H. Balci, and R. L. Greene,
Phys. Rev. Lett. **88**, 207004 (2002).
- ⁵⁵ A. Sharoni, G. Koren, and O. Millo, Europhysics Letters **54**, 675 (2001).
- ⁵⁶ O. Millo and G. Koren, Philosophical Transactions of the Royal Society A: Mathematical,
Physical and Engineering Sciences **376**, 20140143 (2018).
- ⁵⁷ S. Bouscher, Z. Kang, K. Balasubramanian, D. Panna, P. Yu, X. Chen, and A. Hayat, Journal
of Physics: Condensed Matter **32**, 475502 (2020).
- ⁵⁸ S. Kashiwaya, Y. Tanaka, N. Yoshida, and M. R. Beasley, Phys. Rev. B **60**, 3572 (1999).
- ⁵⁹ I. Žutić and O. T. Valls, Phys. Rev. B **60**, 6320 (1999).
- ⁶⁰ J.-X. Zhu and C. S. Ting, Phys. Rev. B **61**, 1456 (2000).
- ⁶¹ T. Hirai, Y. Tanaka, N. Yoshida, Y. Asano, J. Inoue, and S. Kashiwaya, Phys. Rev. B **67**,
174501 (2003).
- ⁶² T. Hirai, N. Yoshida, Y. Tanaka, J.-i. Inoue, and S. Kashiwaya, J. Phys. Soc. Jpn. **70**, 1885
(2001).
- ⁶³ A. Hellenes, T. Jungwirth, J. Sinova, and L. Šmejkal, (2023), arXiv:2309.01607.
- ⁶⁴ S. Ikegaya, J. Lee, A. P. Schnyder, and Y. Asano, Phys. Rev. B **104**, L020502 (2021).
- ⁶⁵ M. Alidoust, C. Shen, and I. Žutić, Phys. Rev. B **103**, L060503 (2021).
- ⁶⁶ F. Yang and M. Wu, Phys. Rev. B **95**, 075304 (2017).

- ⁶⁷ M. Alidoust, Phys. Rev. B **101**, 155123 (2020).
- ⁶⁸ S. H. Jacobsen, J. A. Ouassou, and J. Linder, Phys. Rev. B **92**, 024510 (2015).
- ⁶⁹ J. Lee, S. Ikegaya, and Y. Asano, Phys. Rev. B **103**, 104509 (2021).
- ⁷⁰ X. Liu, J. Jain, and C.-X. Liu, Phys. Rev. Lett. **113**, 227002 (2014).
- ⁷¹ B. A. Bernevig, J. Orenstein, and S.-C. Zhang, Phys. Rev. Lett. **97**, 236601 (2006).
- ⁷² M. Kohda, V. Lechner, Y. Kunihashi, T. Dollinger, P. Olbrich, C. Schönhuber, I. Caspers, V. V. Bel'kov, L. E. Golub, D. Weiss, K. Richter, J. Nitta, and S. D. Ganichev, Phys. Rev. B **86**, 081306 (2012).
- ⁷³ S. Ikegaya, Y. Asano, and Y. Tanaka, Phys. Rev. B **91**, 174511 (2015).
- ⁷⁴ S. Banerjee and M. S. Scheurer, "Altermagnetic superconducting diode effect," (2024), arXiv:2402.14071 [cond-mat.supr-con].
- ⁷⁵ Q. Cheng and Q.-F. Sun, Phys. Rev. B **109**, 024517 (2024).
- ⁷⁶ Y. Tanaka and S. Kashiwaya, Phys. Rev. B **53**, R11957 (1996).
- ⁷⁷ Y. Tanaka and S. Kashiwaya, Phys. Rev. B **56**, 892 (1997).
- ⁷⁸ Y. Tanaka and S. Kashiwaya, Physica C: Superconductivity **274**, 357 (1997).
- ⁷⁹ Y. Tanaka and S. Kashiwaya, Journal of the Physical Society of Japan **69**, 1152 (2000), <https://doi.org/10.1143/JPSJ.69.1152>.